Influence of the Preparation Conditions of Oxidic NiMo/Al$_2$O$_3$ Catalysts on the Sulfidation Ability: A Quick-XAS and Raman Spectroscopic Study

Amélie Rochet,*[†,‡,§] Bertrand Baubet,[†] Virginie Moizan,*[†] Elodie Devers,[†] Antoine Hugon,[†] Christophe Pichon,[†] Edmond Payen,[∥] and Valérie Briois[‡]

[†]IFP Energies nouvelles, Etablissement de Lyon, Rond-point de l'échangeur de Solaize, BP 3, 69360 Solaize, France
[‡]Synchrotron SOLEIL, L'Orme des Merisiers, Saint-Aubin, BP 48, 91192 Gif-sur-Yvette Cedex, France
[∥]Unité de Catalyse et de Chimie du Solide, UMR CNRS 8181, F-59655 Villeneuve d'Ascq Cedex, France

Ⓢ *Supporting Information*

ABSTRACT: The structure of oxidic precursors of supported NiMo hydrodesulfurization catalysts has been investigated in-depth by the combination of laser Raman spectroscopy and X-ray absorption spectroscopy measured at the Mo and Ni K edges at the different stages of the preparation. The oxidic catalysts were prepared by incipient wetness impregnation of δ-alumina with a solution obtained by dissolving MoO$_3$ in H$_2$O$_2$ and subsequently adding Ni(NO$_3$)$_2$·6H$_2$O in this as-prepared solution (8 wt % MoO$_3$; 2 wt % NiO). The formation of the 6-molybdoaluminate Anderson-type hetero-polyanion (AlMo$_6$O$_{24}$H$_6$)$^{3-}$ and of a mixture of oxo−hydroxo nickel species and bulk and/or surface NiAl-layered double hydroxide dispersed at the surface of the support has been identified after drying. Upon further thermal treatment at 723 K under dried air, calcined dehydrated catalyst is constituted of highly distorted isolated or partially condensed tetrahedral Mo units with terminal mono-oxo groups and of bulk and/or surface NiAl$_2$O$_4$-type and NiO-type species. After further exposure of the calcined catalyst to air moisture, a partial recovery of the Anderson-type molybdenum heteropolyanion and NiAl-layered double hydroxide species is evidenced by X-ray absorption spectroscopy. The nature and dispersion of active species formed after sulfidation under H$_2$S/H$_2$ of the different oxidic catalysts (dried-NiMo, dehydrated-calcined NiMo, and calcined-NiMo samples) are finally discussed in light of the structure of the parent oxidic precursors.
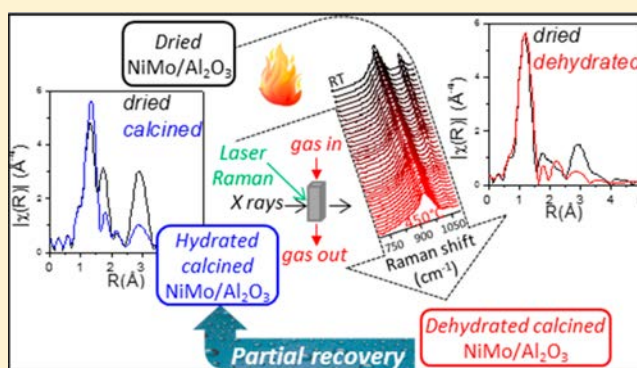
1. INTRODUCTION

The hydrodesulfurization process (HDS), consisting of the catalytic removal of the sulfur heteroelement from diesel and gasoline, is an essential process[1] of the petroleum industry. Because of strengthened environmental regulation concerning the sulfur content in oil fractions, refiners need to produce more efficient HDS catalysts. These latter are commonly based on molybdenum disulfide slabs dispersed on alumina and decorated with cobalt or nickel atoms at the edges and corners of the slabs (described by the mixed active phase with Topsøe's model[2]). The active phase is obtained by sulfiding an oxidic precursor, usually prepared by incipient wetness impregnation of the support using a solution containing Mo and 3d promoter salts, followed by drying. Aqueous solutions of polymolybdates, such as (NH$_4$)$_2$(Mo$_7$O$_{24}$), and of Ni(NO$_3$)$_2$ (or Co(NO$_3$)$_2$) are currently used to prepare industrial HDS catalysts. After impregnation, a calcination pretreatment is carried out in order to eliminate extraneous material present in the precursor salts as volatile components (e.g., NO$_x$ from nitrates) but also, through the transformation of the starting oxomolybdate

species, to improve the dispersion facilitating further sulfidation. Nevertheless, the dehydration of the oxidic precursors occurring upon calcination is recognized to favor the creation of bonds between the support and the oxomolybdate species[3] which slows down the sulfidation activation process. Additionally, it is also well-known that the calcination process can be responsible for the formation of undesirable species such as the spinel-like phases involving Al and promoter atoms[4,5] and/or well-defined Co or Ni molybdate phases which are hardly sulfidable. The balance between the decomposition of oxomolybdates and the interaction of Mo and/or promoter with the support must be carefully controlled since they strongly govern the ability of the catalysts to form the sulfide active NiMoS (or CoMoS) species which will lead to HDS catalysts with high activity. Actually, the understanding of the various stages leading to the preparation

of the oxidic precursors, through an in-depth structural characterization of the species in presence at any stage of the genesis process, has motivated over the years a vast amount of research.[3,6−10] The insight gained on the structure of the oxidic precursors helped to understand the factors that influence the formation of HDS active sites on the support during sulfidation.[11] However, these oxidic precursors were mainly prepared using ammonium heptamolybdate (AHM) precursor solutions.

In this general context and using a new preparation procedure, we carried out an in-depth local order structural characterization by laser Raman spectroscopy (LRS) and X-ray absorption spectroscopy (XAS) of the preparation of a NiMo-based oxidic precursor catalyst at any stage of its preparation, i.e., from its early genesis in solution to the drying stage and subsequent calcination stage. Those local order techniques are well adapted for the *in situ* characterization of supported catalysts.[12,13] The preparation route used herein deals with the dissolution of MoO_3 in an aqueous hydroperoxide solution in which the $Ni(NO_3)_2 \cdot 6H_2O$ is subsequently added. The so-called peroxo route is known to increase the solution stability and solubility of Mo species thanks to the formation of peroxomolybate entities.[14] A recent patent claimed the attractiveness of this route for catalyst preparation,[15] that has been used for the preparation of mixed CoMo heteropolyanions based impregnating solutions.[16,17] A similar hydrogen peroxide route was also proposed for NiMo hydrotreating catalyst preparations,[15] but to the best of our knowledge a detailed characterization of the so-obtained catalysts has not been published.

Aiming to investigate the aforementioned role of calcination, the state of the oxidic catalysts at the different stages of the preparation was characterized, i.e., the dried oxidic catalyst and the calcined one. Since the hydration state of the calcined catalyst was reported as a parameter of paramount importance for the further sulfidation, the calcination treatment under dried atmosphere has been also monitored *in situ* by LRS and Quick-XAS spectroscopy carried out simultaneously at the Mo and Ni K edges. The ability to sulfide the dried catalyst, the calcined one, and the one obtained after calcination without moisture contact has been discussed in light of the local order characterization of the active sulfide phases obtained at the end of the heating process at 673 K in the presence of a mixed H_2S/H_2 atmosphere.

2. EXPERIMENTAL SECTION

a. Catalyst Preparation. The $NiMo/Al_2O_3$-supported catalysts were synthesized by incipient wetness impregnation of a δ-alumina support with a solution of MoO_3 (0.6 M) dissolved into H_2O_2 (3 M) in which nickel nitrate (Fluka) was subsequently added in the 0.5 Ni/Mo molar ratio. The used δ-alumina carrier had a specific surface area of 143 m^2/g and a pore volume of 0.99 mL/g. The metallic content verified by X-ray fluorescence (8 wt % MoO_3 and 2 wt % NiO) resulted in a Mo atomic surface density of 2.3 atoms/nm^2. Following the impregnation step, the solid was matured in a saturated water atmosphere during 12 h in order to ensure a good diffusion of the molybdenum and nickel precursors into the alumina porosity. Then a drying step at 393 K overnight in a static air oven was carried out to obtain the dried NiMo oxidic sample (dried-NiMo).

After the drying step, the catalyst was calcined under air flow (1 L/h) by heating the sample up to 723 K for 2 h with a

heating ramp of 5 K/min. At the end of the calcination, the sample was put in contact with air moisture and stored without any preservation conditions. The calcined NiMo oxidic sample so-obtained is called hereafter calc-NiMo catalyst.

Both dried and calcined catalysts were further sulfided in conditions similar to those described in section 2.b.

After the sulfidation treatment, the dried and calcined sulfided samples were analyzed by transmission electron microscopy (TEM) to determine the average length and stacking of the MoS_2 slabs by counting at least 200 particles. TEM images were taken using a 200 kV JEOL-2010 transmission electron microscope equipped with a digital camera.

b. *In Situ* Catalyst Treatment: Calcination and Sulfidation. The calcination treatment of the dried catalyst was characterized *in situ*. For this purpose, the dried-NiMo catalyst was loaded in the cell available at the hard X-rays SAMBA beamline (SOLEIL, Saint-Aubin) and presented in a previous work.[18] It allows the simultaneous characterization of the catalyst by XAS and LRS under reactive atmosphere and temperature. A mixture of dry O_2 (0.5 mL/min) and dry N_2 (1.6 mL/min) was flowed through the dried-NiMo catalyst heated up to 723 K for 2 h with a rate of 2 K/min. Then the as-obtained sample was cooled down at room temperature (RT) under the same dried gas mixture. At the end of the treatment, keeping the sample preserved from air moisture, the so-called dehydrated-calc-NiMo catalyst was sulfided in the same conditions as the dried and calcined catalysts.

The three oxidic NiMo samples (i.e., dried-NiMo, calc-NiMo, and dehydrated-calc-NiMo) were sulfided in the catalytic cell[18] by raising the temperature at a rate of 2 K/min from RT to 673 K under a flow of a mixture of 15% of H_2S into H_2 at atmospheric pressure (2 mL/min with 50 mg of powdery catalyst). After reaching 673 K, the catalyst was maintained under sulfiding atmosphere for 2 h. The different sulfide catalysts are called hereafter dried-sulf-NiMo, calc-sulf-NiMo, and dehydrated-calc-sulf-NiMo.

c. LRS Characterization. *Ex situ* LRS spectra of the samples were recorded from 100 to 1100 cm^{-1} using the exciting line at 532 nm of a diode pumped solid state laser. An Invia Raman (Renishaw) spectrometer with a 2400 lines·mm^{-1} grating was used for the characterization of the impregnating solutions and wet precipitate whereas a LabRam ARAMIS (HORIBA Jobin-Yvon) spectrometer with a 1800 lines·mm^{-1} grating was used for the spatially resolved characterization of the dried-NiMo sample and the calc-NiMo one (spot size 2 μm). Measurements at several positions on the samples, called hereafter position of interest (POI), were carried out in order to check the homogeneity of the dried-NiMo and calc-NiMo samples. Whatever the spectrometer, the laser beam was focused with a long working distance 50× objective. The laser power used was 70 mW for the solution and 5 mW for the catalysts. The measurements were achieved under ambient conditions.

Moreover, the calcination treatment was monitored *in situ* by combining Quick-XAS and LRS measurements. LRS spectra were recorded with a Raman RXN1 spectrometer (Kaiser Optical Systems, Inc. (KOSI)) using an excitation laser line at 532 nm. A highly sensitive CCD detector coupled with the Holoplex transmission dispersive grating provided fast and simultaneous full spectral collection of Raman data from 200 to 4250 cm^{-1}. The average resolution was 2 cm^{-1}. The laser beam was focused with a 140 mm long working distance objective
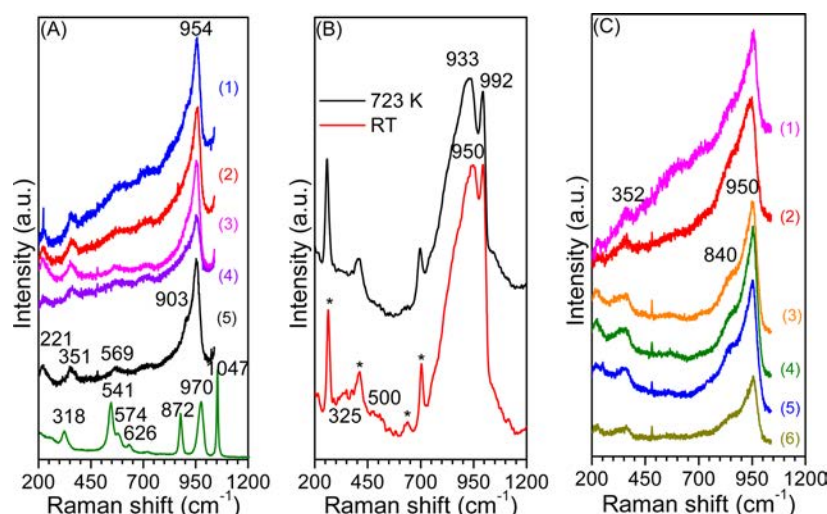
Figure 1. (A) RT Raman spectra of the impregnating solution (green) and of the powdery dried-NiMo catalyst at different positions of interest (POIs) numbered from (1) to (5). (B) Raman spectra of the dehydrated-calc-NiMo sample measured at 723 K (black) and at RT after subsequent cooling down without contact to air moisture (red). The peaks marked by a star symbol are due to the mica window. (C) RT Raman spectra of the calc-NiMo catalyst recorded at different POIs numbered from (1) to (6).

($\times$10 magnification). In order to allow the *in situ* Raman measurements, the catalytic cell (from ref 18) was equipped with a mica window facing the incoming laser. The laser power measured at the cell position was 11 mW. The integration time for one spectrum was set to 30 s, and the data presented for the calcination process were the average of 4 spectra of 30 s.

d. XAS Characterization. *i. XAS Measurements.* The dried oxidic sample (dried-NiMo) and the calcined one (calc-NiMo) were carefully characterized by *ex situ* Mo K edge and Ni K edge EXAFS (extended X-ray absorption fine structure). The measurements were done on the powdery sample at low temperature (using liquid nitrogen or helium cryo-cooling) in the so-called high flux mode available on the SAMBA beamline (SOLEIL) using the sagitally focusing Si(220) monochromator.[19]

The calcination of the dried-NiMo sample was investigated *in situ* by following the Mo K edge and the Ni K edge in the so-called time-resolved Quick-XAS mode.[19] XAS measurements were carried out using the edge jumping capability of the double Quick-XAS channel-cut monochromator[20] of the SAMBA beamline.[19] This permits the alternate characterization at both edges of bimetallic heterogeneous catalysts by using as monochromator either the Si(111) or the Si(311) channel-cut crystal. For both edges a frequency of 1 Hz was used for the crystal oscillation allowing the measurement of two spectra per second (one for increasing energies, the other one for decreasing energies). Consecutive spectra (with increasing energy), collected during 1 min at each edge, were merged to improve the signal-to-noise ratio.

Moreover, the dried-sulf-NiMo, calc-sulf-NiMo, and dehydrated-calc-sulf-NiMo samples were characterized in Quick-XAS mode after the *in situ* sulfidation treatment. XAS and LRS *in situ* monitoring upon the sulfidation process will be discussed in a forthcoming paper.

For the whole measurements, XAS spectra were measured in transmission mode with three ionization chambers (IC) as X-ray detectors. The ICs were filled with argon for measurements at the Mo K edge and with nitrogen for those at the Ni K edge.

ii. XAS Data Handling. Analysis of the XANES (X-ray absorption near edge structure) data was performed by using the Athena graphical interface program.[21] The energy was calibrated to the first inflection point of a Ni or Mo metal foil defined at 8333 and 20003.9 eV, respectively. Then the spectra were background corrected and normalized using the flattening algorithm used by Athena.

Mo K Edge. $k^3\chi(k)$ EXAFS signals collected at 77 K and/or RT were Fourier transformed in R-space pseudoradial distribution functions using a Kaiser–Bessel window between $k_{min} = 4.5$ Å^{-1} and $k_{max} = 13.8$ Å^{-1} and dk window sill parameter equal to 2. For the sulfide samples, FT of the $k^3\chi(k)$ EXAFS data recorded at 673 K were carried out between 3.5 and 12.5 Å^{-1} with a dk parameter of 2.

Ni K Edge. FT of the $k^3\chi(k)$ EXAFS data recorded at 20 K and/or RT were carried out from 3.3 to 11 Å^{-1} with a dk parameter equal to 2. For the sulfide samples, FT of the $k^3\chi(k)$ EXAFS data recorded at 673 K were limited in the 3−9.5 Å^{-1} k range.

It is noteworthy that Fourier transforms presented in the figures are not phase corrected. Then the distances of the main FT contributions which are discussed in the text are shifted compared to the real crystallographic distances. Fits of EXAFS spectra were performed by using the Artemis graphical interface program[21] based on *ab initio* phase and amplitude calculated by the FeFF6 code.[22] References, prepared as pellets and recorded in the same conditions as the catalysts, were used to determine S_0^2 (the passive electron reduction factor) and enot (energy shift) parameters, which are then transferred to the fit of the samples. Structural parameters R (average atomic distance from the emitting atom), N (coordination number), and σ^2 (Debye–Waller factor) were determined by least-squares fitting procedures using a multiple k-weight data procedure. Defined by the IXS standards and criteria committee and available at http://ixs.iit.edu/subcommittee_reports/sc/err-rep.pdf, the goodness of fit is given by the minimum value of the statistical χ^2 metric parameter and of the reduced χ^2 quality factor defined as the ratio of χ^2 over ν (where $\nu = N_{ind} - N_{var}$ with N_{ind} the number of free parameters allowed to vary in a fit and N_{var} the number of variables used in the model). The χ_ν^2 parameter obtained for each fit and the R_F-factor, which measures the relative misfit with respect to the experimental

data, are reported in the tables. The number of free parameters allowed to vary in the fit depends on the k range of the Fourier transforms and the R range used for the inverse Fourier transforms. In this paper, N_{ind} is equal to 14 for Mo K edge fittings, 10 for Ni K edge fitting of oxidic species, and 6 for Ni K edge fitting of sulfide species.

iii. Multivariate Curve Resolution Analysis. During thermal treatment under controlled atmosphere, complex chemical transformations involving several unknown species can occur. As successfully reported in several recent time-resolved XANES studies,[23−29] the identification of the phases present during the *in situ* treatment can be obtained using the MCR-ALS (multivariate curved regression with alternative least squares) chemometric method. A comprehensive detailed description of the MCR-ALS methodology applied to XAS can be found in refs 23,26,28. The MCR-ALS minimization algorithm, developed under Matlab 6.5 by the group of R. Tauler,[30] was used herein for isolating, from the corresponding experimental data set, the spectra of the nickel species formed upon *in situ* calcination. A least-squares combinatorial fitting of the XANES spectra recorded at the Ni K edge after calcination and using the spectra of the chemical species previously identified and isolated as pivotal compounds by MCR-ALS was carried out using the Athena software.[21]

e. Reference Compounds. The inorganic compounds used as references for XAS or LRS characterizations are issued from previous works or are commercial compounds. Their synthesis and verification are described in the corresponding published works for respectively 6-molybdoaluminate Anderson-type heteropolyanion[9] and NiAl-based layered double hydroxide.[31] Commercial standards have been used for $Ni(NO_3)_2 \cdot 6H_2O$, NiO, MoO_3, MoS_2 (Sigma-Aldrich), $Al_2(MoO_4)_3$ (Alfa Aesar), $NiAl_2O_4$ (Pharmacie Centrale de France), and Ni_3S_2 (Strem).

3. RESULTS

a. Characterization of the Different Oxidic Catalysts.
i. LRS Characterization. Raman spectra of the as-prepared catalysts and the impregnating solution used for the sample preparation are presented in Figure 1.

Dried-NiMo Catalyst. Figure 1A displays the Raman spectra of the fresh impregnating solution and of the powdery dried-NiMo oxidic sample at different spatial positions of interest (POIs). The Raman spectrum of the solution resulting from the dissolution of MoO_3 in H_2O_2 in which $Ni(NO_3)_2 \cdot 6H_2O$ was subsequently added displays the intense line at 1047 cm^{-1} characteristic of the symmetric stretching vibrational mode of the nitrate anions introduced with the promoter.[32] The lines at 970, 872, 626, 574, 541, and 318 cm^{-1} are ascribed to the peroxodimolybdenum entities $(Mo_2O_3(O_2)_4^{2-})$.[16] These lines are respectively assigned to the stretching mode of the terminal $M=O_t$, the peroxo O−O, the Mo−O−Mo bridge, and the Mo−(O_2) moieties (asymmetric and symmetric) and to the deformation mode of Mo−O_t vibration.[16] The line at 872 cm^{-1} may also correspond to the excess of hydrogen peroxide.[33] However, the invariance of the lines during aging (Figure S1) strongly suggests that this line only corresponds to the O−O stretching mode of the peroxomolybdenum species.[34]

As displayed in Figure 1A, the features ascribed to the presence of $Mo_2O_3(O_2)_4^{2-}$ entities are no longer observed upon deposition on alumina, whatever the spatial positions of interest of the dried-NiMo sample surface. The POIs present a common fingerprint indicating that the species are homoge-neously distributed at the surface of the alumina and are different from the ones observed for the solution (green curve, Figure 1A). It is noteworthy that the dissolution of MoO_3 was complete since no characteristic line of this oxide has been identified by Raman[35] either in solution or in the dried-NiMo sample. The Raman spectra of the dried-NiMo catalyst exhibit a broad line at 954 cm^{-1} with a shoulder at 903 cm^{-1}, respectively assigned to the symmetric and asymmetric stretching mode of terminal Mo=O_{2t} bond of dioxo cores of alumina supported oxomolybdate species.[35,36] Additional lines are also observed at 569, 351, and 221 cm^{-1}. The line at around 350 cm^{-1} is associated with the deformation modes of the terminal Mo=O_{2t} groups whereas the line around 220 cm^{-1} is assigned to the deformation modes of the bridging Mo−O−Mo bonds.[10,37] It is worth to note that the simultaneous presence of Raman lines at 954, 903, and 569 cm^{-1} is usually used as a fingerprint for the presence of the 6-molybdoaluminate Anderson-type heteropolyanion $(AlMo_6O_{24}H_6)^{3-}$, hereafter noted $[AlMo_6]$,[9] the line at 569 cm^{-1} being characteristic of the Al−O(−Mo) stretching vibrational mode.[3] The Raman spectrum observed for the dried-NiMo catalyst can thus be associated with the formation of $AlMo_6$ heteropolyanion.[3]

Dehydrated-calc-NiMo Catalyst. Figure 1B shows the Raman spectra of the dehydrated-calc-NiMo catalyst obtained after *in situ* calcination (see section 3.b) without contact to air moisture. The spectra are recorded at 723 K under dried air and after cooling down at RT. The peaks marked by a star symbol are due to the mica window (as shown with the spectrum of the mica window presented in Figure S2). A well-defined line at 992 cm^{-1} is systematically observed with a broad underlying shoulder in the low wavenumber range extending from 750 to 950 cm^{-1}.[38] The broad underlying band is generally assigned to the asymmetric stretching mode of the Mo−O−Mo bridge and to the bridging Mo−O(−Al) stretching mode of the bonds with the support.[35,39] The position of both lines and their intrinsic intensity ratio (I_{992}/I_{840}) have been shown to be strongly dependent on the Mo loading[39] but also on the dehydration rate.[40] The broad underlying line and the high wavenumber one evolve with the temperature of dehydration. This suggests, in agreement with the Mo loading, the presence of more or less polymeric dehydrated entities that are linked to the support. This also explains the evolution of the spectrum upon cooling down at RT. Indeed the intensity maximum of the broad line recorded for the dehydrated-calc-NiMo catalyst shows an upward shift from 933 to 950 cm^{-1} upon cooling as a result of a partial rehydration by the hydroxyl groups of the alumina support.

According to the literature, the high wavenumber line, herein located at 992 cm^{-1}, is assigned to the symmetric stretching vibrational mode[40] of mono-oxo terminal (Mo=O_t groups) of MoO_x species bonded to the surface.[40−42] At the Mo loading considered in this work, Wachs et al.[41] suggested the formation upon dehydration of a polymeric structure linked to the support with $O_5Mo=O_t$ distorted octahedral units. Molybdenum is a versatile element that can adopt various configurations between pure tetrahedral and pure octahedral environment with a number of terminal Mo=O_t bonds that depends on the way the polyhedrons are linked together, i.e., edge or corner sharing. The position of the terminal Mo=O_t stretching line is thus strongly dependent on the geometry of these polyhedrons, the Mo being always in an oxygen environment between tetrahedral and octahedral.[43] Actually, the high wavenumber line at 992 cm^{-1} is assigned to the symmetric stretching

vibrational mode of terminal mono-oxo group in highly distorted Mo environment as in α-MoO$_3$[44,45] or aluminum molybdate.[46] Considering that, in α-MoO$_3$, the polyhedrons consist of 1 O at 2 short distances (at 1.67 and 1.73 Å), 2 O at intermediate ones (1.95 Å), and 2 O at long distances (2.25 and 2.33 Å), Raman spectroscopic results lead us to propose, at this Mo coverage (2.3 atoms/nm^2), the formation upon calcination of highly distorted tetrahedral Mo units with terminal mono-oxo group, which are isolated and/or inserted in polymolybdate entities both being linked to the support. This is in agreement with a recent paper of Tsilomelekis et al. in which they discussed the assignment of the Raman lines to the different Mo cores that may exist on various supports.[47]

Calcined-NiMo Catalyst. The spectra recorded at different POIs of the calc-NiMo sample after contact to air moisture are presented in Figure 1C. Contrary to the observation for the dried-NiMo catalyst, the spectra of the different POIs slightly differ, suggesting some heterogeneities in the evolution of the surface species upon rehydration during transfer in air after calcination. Irrespective of the positions, the line at 992 cm^{-1}, which was a characteristic fingerprint of the dehydrated state of the catalyst after calcination (before further contact with air moisture), is no more observed on the spectra presented Figure 1C. Actually, the characteristic lines of the calc-NiMo catalyst are located around 950, 840, and 352 cm^{-1}. The relative intensity of the lines at 950 and 840 cm^{-1} evolves depending on the explored POIs. The spectra recorded at POI 2 and POI 5 display a more intense broad line at 840 cm^{-1} than the other ones. Those reported at other positions have a shape more related to the shape characterizing the AlMo$_6$ species. This suggests that the AlMo$_6$ entities are recovered upon transfer in the air moisture, but this reversibility is far from complete in our experimental conditions.

ii. Mo K Edge XAS Characterization. Mo K edge XANES spectra and Fourier transforms obtained for the catalysts and references are presented in Figure 2A and Figure 2B, respectively. The position of the rising edge in the XANES spectra of the catalysts presented in Figure 2A is characteristic of hexavalent molybdenum species as deduced from the comparison with spectra of standard references. All the samples display a pre-edge feature arising from transition from 1s toward molecular orbitals in which 4d Mo orbitals are hybridized with p Mo orbitals due to the presence of a non-centrosymmetric environment for Mo.[48] As a matter of fact, the contribution of oxygen atoms located between 1 and 2 Å in the FT of the catalysts presented in Figure 2B displays several resolved peaks with evolving intensity depending on the catalyst treatment. This indicates modification of the local order around Mo throughout the drying and calcination processes. In the following, specific results gained for each catalyst will be presented.

Dried-NiMo Catalyst. On one hand, the XANES spectrum of the dried-NiMo sample presented as curve (a) in Figure 2A is very similar to the one of the reference corresponding to the 6-molybdoaluminate ammonium salt (Figure 2A, (f)), a finding that is totally in agreement with the Raman results (Figure 1A).

On the other hand, the comparison of the Fourier transforms of the dried-NiMo catalyst and of the AlMo$_6$ reference (Figure 2B) together with the corresponding in-phase EXAFS oscillations (Figure S3), clearly confirms the formation of this Anderson-type species observed by Raman spectroscopy. The large distribution of Mo−O distances in the first coordination shell suggested by the observed pre-edge intensity is fully
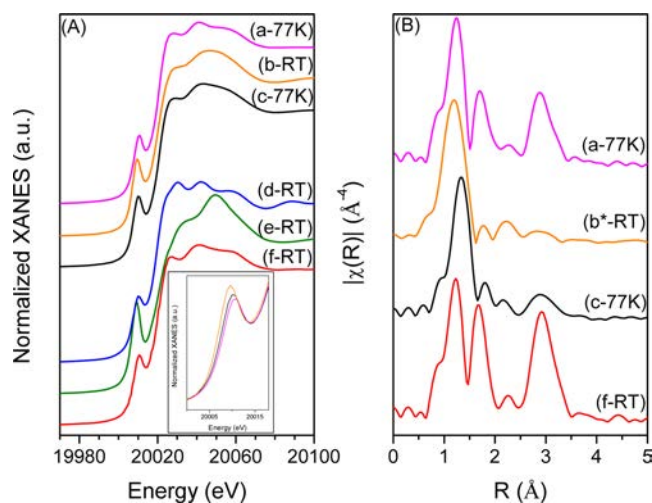

Figure 2. (A) Mo K edge XANES of the catalysts and references: (a) dried-NiMo (77 K); (b) dehydrated-calc-NiMo (RT); (c) calc-NiMo (77 K); (d) MoO$_3$ (RT); (e) Al$_2$(MoO$_4$)$_3$ (RT); (f) AlMo$_6$ (RT). (B) Fourier transform moduli of the catalysts and references: (a) dried-NiMo (77 K); (b*) dehydrated-calc-NiMo (RT); (c) calc-NiMo (77 K); (f) AlMo$_6$ (RT). FTs are obtained with a k-range between 4.5 and 13.8 Å^{-1}. The one marked with a star symbol is obtained with a narrower range (3.0−10.5 Å^{-1}).

Table 1. Mo K Edge Fit EXAFS Parameters of the Dried-NiMo (77 K), Dehydrated-calc-NiMo (RT), and Calc-NiMo (77 K) Catalysts

backscatterer	N	R (Å)	σ^2 (Å^2) $\times$ 10^3	R-factor	χ_ν^2
		Dried-NiMo, Fit A (77 K)			
O	2.6 ± 0.2	1.72 ± 0.01			
O	1.2 ± 0.4	1.96 ± 0.01			
O	1.5 ± 0.3	2.28 ± 0.02			
Al	0.6 ± 0.3	2.65 ± 0.03	3.2 ± 4.6	0.0017	349
Mo	1.2 ± 0.4	3.30 ± 0.01			
Al	1.0 ± 0.5	3.40 ± 0.06			
Δk = 4.5–13.8 Å^{-1}, S_0^2 = 0.8, E_0 = 20020.66 eV, enot = −5.01 eV					
		Dehydrated-calc-NiMo, Fit B (RT)			
O	4.3 ± 1.2	1.75 ± 0.01	8.6 ± 2.9	0.0011	70
Δk = 3.0–10.5 Å^{-1}, S_0^2 = 0.8, E_0 = 20020.66 eV, enot = −5.01 eV					
		Calc-NiMo, Fit C (77 K)			
O	2.4 ± 0.2	1.74 ± 0.01			
O	0.7 ± 0.2	2.30 ± 0.02			
Al	0.5 ± 0.2	2.67 ± 0.02	2.6 ± 0.6	0.0026	189
Mo	0.6 ± 0.2	3.30 ± 0.03			
Mo	0.4 ± 0.2	3.42 ± 0.04			
Δk = 4.5–13.8 Å^{-1}, S_0^2 = 0.8, E_0 = 20020.66 eV, enot = −5.01 eV					

confirmed by the structural parameters determined by the EXAFS fits (Table 1, Figure S4A). The shortest Mo−O bonds (1.72 ± 0.01 Å) are ascribed to terminal Mo=O$_t$ bonds, the other longer Mo−O bonds being bridging Mo−O−Mo ones. The best fit for the contribution of neighbors located on the FT around 3 Å characterizing the dried-NiMo sample (Figure 2B, FT (a)) is obtained by using a Mo−Al contribution at ∼3.40 Å together with a Mo−Mo contribution at ∼3.30 Å, as expected for the AlMo$_6$ structure (fit A in Table 1 and Figure S4A). It is noteworthy that tentative fittings with a Mo−Ni contribution instead of the Mo−Al ones were unsuccessful. This is an indication that 6-molybdonickelate entities, analogue of the AlMo$_6$ one in which the central atom is Ni, are probably not

formed during the preparation of the oxidic precursor. Finally, interactions between the support and molybdenum species are evidenced by the presence of a Mo–Al path contribution at 2.65 (0.06) Å which is necessary to include in the fit of the dried-NiMo sample to obtain the lower statistical fitting χ_ν^2 metric together with a smaller value of R_F-factor (without this contribution the fit results in $R_F = 0.0105$, $\chi_\nu^2 = 805$, not shown here). Interaction between the support and oxomolybdate species have been already suggested from Raman[3] and EXAFS results.[49] For the latter technique, the distance between Mo and the Al atom of a γ-alumina support ranges from 2.72 to 2.76 Å. The slight difference in distance can be ascribed to the constrained fits used herein for the EXAFS refinement with a unique Debye–Waller factor for all the contributions. This constraint is due to the fact that the limited number of independent points in the experimental data ($N_{ind} = 14$) determines the upper number of parameters that can be refined (herein $N_{var} = 13$ parameters were refined for fit A).

Dehydrated-calc-NiMo Catalyst. The RT XANES spectrum of the dehydrated-calc-NiMo catalyst presented in curve (b) in Figure 2A is characterized by a featureless shape compared to the spectra of dried-NiMo catalyst (77 K) or of the AlMo$_6$ reference (RT) with in particular a single resonance centered at ~20049 eV together with an increase of the pre-edge intensity (well shown in the inset of the figure). The increase of the pre-edge intensity is usually interpreted as an increase of the proportion of non-centrosymmetric molybdenum polyhedra.[48] This is in agreement with the shape of the broad white line which becomes very similar to that recorded for tetrahedral molybdenum oxo species like in Na$_2$MoO$_4$[50] suggesting the formation of tetrahedral Mo environments in agreement with the Raman results.

The Fourier transform of the Mo K edge EXAFS data recorded at RT for the catalyst after its calcination without being exposed to air is shown in Figure 2B (FT (b*)). Due to the lower quality of the EXAFS spectrum recorded at RT for the dehydrated-calc-NiMo catalyst compared to those recorded at 77 K for the dried-NiMo and calc-NiMo samples, the *k*-window range for the Fourier transform is limited in the 3.0–10.5 Å^{-1} *k*-range. This reduced *k*-range hinders further quantitative least-squares fitting of the EXAFS data for the dehydrated-calc-NiMo sample beyond the first coordination shell (fit B in Table 1 and Figure S4B). This latter is satisfactorily reproduced by 4.3 (1.2) oxygen atoms at 1.75 (0.01) Å ($R_F = 0.0011$, $\chi_\nu^2 = 70$). Nevertheless, the comparison of the FT of the dehydrated-calc-NiMo catalyst with the contribution of single scattering Mo–Al and Mo–Mo paths used for fitting the dried-NiMo sample suggests that the Mo–Al and Mo–Mo contributions still exist for the dehydrated-calc-NiMo sample (see Figure S5). Indeed, the contribution centered on the FT around 2.3 Å remains remarkably present in the FT suggesting that, after calcination, the oxomolybdate species still presents interactions with the support (as before the calcination treatment). However, the decrease of the intensity of the Mo–Mo contributions located between 2.5 and 3.4 Å on the FT, observed after calcination, confirms the observation made by Raman after calcination treatment and air-moisture preservation showing the decomposition of the AlMo$_6$ deposited molybdenum entities toward less condensed oxomolybdenum species.

Calcined-NiMo Catalyst. The pre-edge intensity of the 77 K XANES spectrum of the calc-NiMo catalyst presented in curve (c) in Figure 2A is intermediate compared to those displayed

for the dried-NiMo and dehydrated-calc-NiMo (see inset in Figure 2A) whereas the main resonance shape appears less structured than the one observed for the dried-NiMo and flatter than the one reported for the dehydrated-calc-NiMo. All these findings suggest further modifications of the local order around Mo upon air moisture exposure.

The Fourier transform of the calc-NiMo catalyst (Figure 2B, FT (c)) displays medium range order contributions of lower intensity than the dried-NiMo catalyst (Figure 2B, FT (a)). Nevertheless the different contributions in the 2.5–3.4 Å range appear in phase with those recorded for the dried-NiMo catalyst suggesting in agreement with the LRS results that the Anderson-type AlMo$_6$ molybdate species is partially recovered after exposure to air moisture. The structural parameters (Table 1, fit C, and Figure S4) are in agreement with the partial recovery of the Anderson-type polyanion upon exposure to air moisture. Nevertheless, the decrease of coordination numbers for the Mo–O and Mo–Mo/Mo–Al contributions is consistent with a mixture of tetrahedral Mo units and Anderson-type heteropolyanions. Finally, it is important to note the presence of the Mo–Al contribution at 2.67 (0.02) Å, which indicates that the molybdate species are still in interaction with the support after calcination treatment and contact with air moisture.

iii. Ni K Edge XAS Characterization. Ni K edge XANES spectra and corresponding FT obtained for the catalysts and references are presented in Figure 3A and Figure 3B,
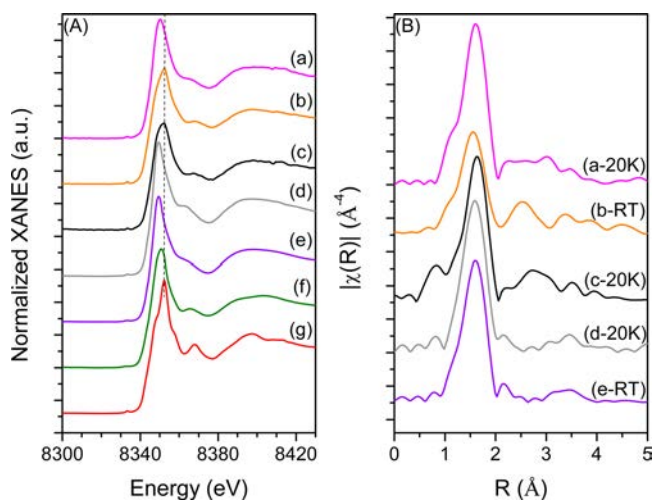

Figure 3. (A) Ni K edge RT XANES of the catalysts and references: (a) dried-NiMo; (b) dehydrated-calc-NiMo; (c) calc-NiMo; (d) nickel(II) nitrate hexahydrate; (e) aqueous solution of nickel nitrate; (f) NiAl-LDH; (g) NiAl$_2$O$_4$. (B) Fourier transform moduli of the catalysts and references: (a-20K) dried-NiMo; (b-RT) dehydrated-calc-NiMo; (c-20K) calc-NiMo; (d-20K) nickel(II) nitrate hexahydrate; (e-RT) aqueous solution of nickel nitrate.

respectively. Although the rising edge position of the XANES spectra of the different catalysts is consistent with the presence of divalent nickel species whatever the treatment of the samples, remarkable change of the positions of the maximum of the white line is observed in the XANES spectra of the different catalysts. The Fourier transforms of the three catalysts are characterized by a main contribution located at ~1.5 Å corresponding to the first oxygen coordination shell and to a broad contribution between 2 and 4 Å with slight differences depending on the catalyst treatment. As for the Mo K edge

Table 2. Ni K Edge Fit EXAFS Parameters of the Dried-NiMo (20 K), Dehydrated-calc-NiMo (RT), and Calc-NiMo (20 K) Catalysts[a]

backscatterer	N	R (Å)	σ^2 (Å^2) × 10^3	R-factor	χ_ν^2
		Dried NiMo, Fit D (20 K)			
O	5.8 ± 0.4	2.07 ± 0.01	3.6 ± 2.8		
Al	2.6 ± 1.4	3.08 ± 0.05	1.0 ± 15.9	0.0174	378
Ni	2.6 ± 1.6	3.07 ± 0.04	5.5 ± 13.5		
		Dehydrated-calc-NiMo, Fit E (RT)			
O	5.2 ± 0.5	2.03 ± 0.01	7.3 ± 1.7		
Al	2.3 ± 1.1	2.89 ± 0.04	13.2 ± 9.1	0.0035	28
Ni	1.1 ± 0.7	3.01 ± 0.05	12.4 ± 9.3		
		Calc-NiMo, Fit F (20 K)			
O	5.4 ± 0.4	2.06 ± 0.01	3.5 ± 2.5		
Al	2.6 ± 1.4	3.07 ± 0.06	9.4 ± 1.1	0.0071	186
Ni	3.0 ± 1.4	3.08 ± 0.03	9.4 ± 1.1		

[a] Δk = 3.3−11 Å^{-1}, S_0^2 = 0.8, E_0 = 8348 eV, enot = −2.79 eV.

results, specific results gained for each catalyst will be presented in this section.

Dried-NiMo Catalyst. Ni K edge RT XANES data recorded for the dried-NiMo catalyst (Figure 3A, (a)) is compared to the spectrum of an aqueous solution of nickel nitrate (0.2 M) (curve (e)) and to the spectrum of a Ni(NO$_3$)$_2$·6H$_2$O reference (curve (d)). The intense white line located at 8350.3 eV and the small pre-edge displayed by these three spectra are characteristic of a nickel atom in an oxygen octahedral environment.[51] Nevertheless the XANES spectrum of the dried-NiMo catalyst (Figure 3A, (a)) is not superimposable either with the spectrum of the aqueous solution of nickel nitrate (Figure 3A, (e)) or with the one of the Ni(NO$_3$)$_2$·6H$_2$O pellet (Figure 3A, (d)), suggesting that upon impregnation the local order around Ni has been modified compared to the solution or to the salt used for catalyst preparation.

The Fourier transform of the Ni K edge EXAFS data recorded for the dried-NiMo catalyst at 20 K displays a broad contribution of neighbors between 2 and 4 Å (Figure 3B, FT (a)). If the contribution centered around 3.5 Å can be ascribed as having the same origin as the contribution observed for the Ni(NO$_3$)$_2$·6H$_2$O pellet which mainly results from multiple scattering events within the first coordination shell made of 6 water molecules,[52] the contributions at shorter distances have a different origin. As gathered in Table 2, fit D (and Figure S4B), the least-squares fitting of the Ni K edge EXAFS signal recorded for the dried-NiMo catalyst reveals that this contribution of neighbors is made of Ni−Ni and Ni−Al contributions at the same distance ∼3.08 Å, suggesting the formation of a phase involving Ni and Al atoms. The distances found as second metallic neighbors are in agreement with the formation of NiAl-based layered double hydroxide (LDH) phase (Ni−O at 2.05 Å, Ni−Ni and Ni−Al at 3.08 Å)[53,54] as bulk and/or surface phases. A satisfactory linear combination fitting (LCF) of the RT Ni K edge XANES spectrum of the dried-NiMo catalyst is achieved with the RT Ni K edge EXAFS spectrum of the nickel nitrate aqueous solution (∼67%) and the RT Ni K edge EXAFS spectrum of a NiAl-based LDH phase (∼33%)[31] (see Figure S6 and Table S1). This result can be considered as a confirmation of the presence of a mixture of oxo−hydroxo nickel species [noted hereafter Ni(H$_2$O)$_x$(OH)$_y$ with x + y = 6] and of a bulk and/or surface NiAl-LDH. Finally it is noteworthy that, with the preparation method and precursors used herein, interaction between the molybdenum

and the promoter, if existing, is not a large contributor to the EXAFS signal, on the dried-NiMo catalyst.

Dehydrated-calc-NiMo Catalyst. The Ni K edge XANES spectrum of the dehydrated-calc-NiMo catalyst presented in Figure 3A (curve (b)) displays a significant energy shift of the white line (8352.4 eV) compared to the white line of the dried-NiMo catalyst (8350.3 eV) together with a reduction of its intensity. The position of the white line of the dehydrated-calc-NiMo catalyst is close to the position of the white line of the NiAl$_2$O$_4$ reference (8352.0 eV). These findings point out structural modifications suffered by nickel upon calcination without air moisture contact.

Figure 3B (FT (b)) presents the Fourier transform of the RT Ni K edge EXAFS data for the oxidic precursor after *in situ* calcination (dehydrated-calc-NiMo). The structural parameters determined by least-squares fitting of the EXAFS data are gathered Table 2, fit E. Compared to the dried-NiMo sample, a lower value of the mean coordination number for the first Ni−O contribution is determined by fitting whereas the second contribution of neighbors is located at shorter distances (Table 2, fit E). Actually, this latter contribution is reproduced in the fit by introducing a Ni−Al at 2.89 (0.04) Å and a Ni−Ni contribution at 3.01 (0.05) Å (Figure S4B). It is noteworthy that the Ni−Al contribution at 2.89 (0.04) Å is in good agreement with the structure of NiAl$_2$O$_4$.[55] This finding together with the shift of the white line in a position close to the one reported for the spectrum of NiAl$_2$O$_4$ strongly suggests that the dehydrated-calc-NiMo is composed of nickel aluminate based species, but only partly since the crystallographic structure related to the nickel aluminate phase does not explain the Ni−Ni contribution at 3.01 Å.

Calcined-NiMo Catalyst. After exposure to air moisture, the position of the white line of the Ni K edge XANES spectrum of the calc-NiMo catalyst, presented in Figure 3A, curve (c), shows a slight reverse shift compared to the one observed after calcination of the dried-NiMo catalyst to form the dehydrated-calc-NiMo catalyst. The position of the white line is located at an intermediate energy value (8351.7 eV) compared to the white line of the dried-NiMo catalyst (8350.3 eV) and the one of the dehydrated-calc-NiMo catalyst (8352.3 eV), indicating again that nickel species are transformed after calcination and subsequent exposure to air moisture. Fourier transform of the EXAFS data recorded at 20 K for the calc-NiMo catalyst is presented in Figure 3B (curve c), and parameters of fits are reported in Table 2 (fit F) (Figure S4B). The Fourier transform
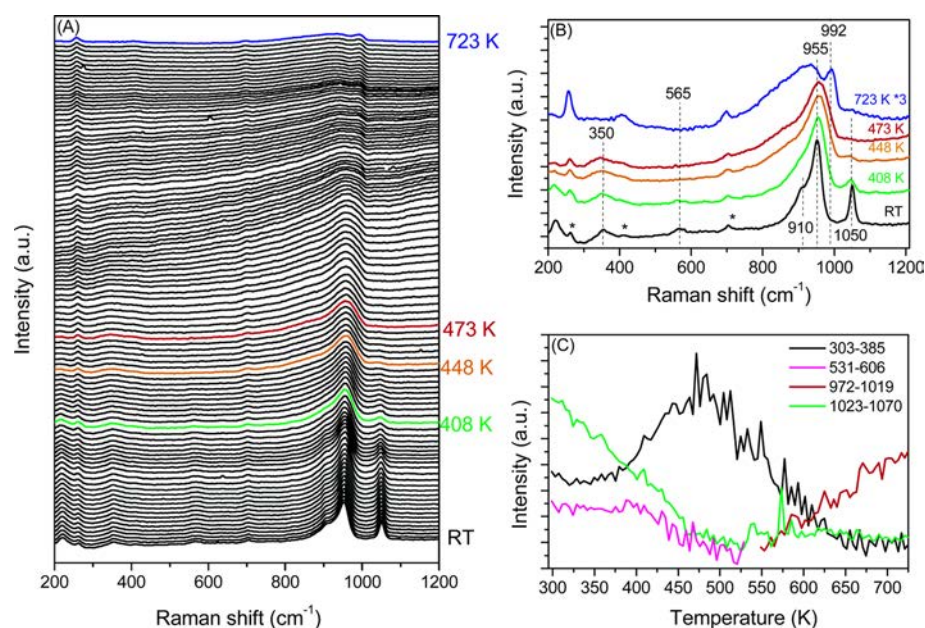
Figure 4. *In situ* monitoring of the calcination of the dried-NiMo catalyst by LRS (A, B) with reports of the evolution of integrated intensity of some specific LRS bands (C). In panel B, the spectrum recorded at 723 K has been multiplied by a factor 3.

of the calc-NiMo sample (Figure 3B, FT (c)) appears very similar to the one measured on the dried-NiMo catalyst (FT (a)). As a matter of fact, the structural parameters gathered for both catalysts in Table 2 (fit D and fit F) are very close, suggesting that upon exposure to air moisture the NiAl-LDH species is partially recovered. Nevertheless the XANES spectrum of the NiAl-LDH phase is not completely superimposable with the one of the calc-NiMo catalyst, suggesting that additional phase enters in the composition of this catalyst. Finally it is noteworthy that, with the preparation method and precursors used herein, no interaction between the molybdenum and the promoter has been evidenced (with the used technique) after calcination.

To go further in the characterization of both dehydrated-calc-NiMo and calc-NiMo catalysts and in particular to determine the nature of the unknown species, we investigate in depth the calcination process using combined LRS and Quick-XAS measurements.

b. In Situ Calcination of the Dried-NiMo Catalyst. i. LRS Characterization. The LRS spectra recorded upon calcination in the *in situ* cell are presented in Figure 4A. The positions of the lines recorded *in situ* for the dried-NiMo catalyst are in good agreement with those measured *ex situ* and presented in Figure 1A, i.e., within the frequency resolution of both spectrometers. For the sake of clarity, some spectra recorded at characteristic temperatures are compared in Figure 4B, whereas the integrated areas of some characteristic bands discussed below are plotted as a function of the cell temperature in Figure 4C. The lines marked with a star are due to the mica window, as shown by the comparison of the spectrum of the dried-NiMo catalyst with the spectrum of the mica window (see Figure S2).

Upon increasing temperature the first striking modification observed on the LRS data arises around 323 K and is related to the decomposition onset of the nitrate groups. Namely, above this temperature, an intensity decrease of the line characteristic of the nitrate ions at 1050 cm^{-1} is clearly evidenced with the decrease of the integrated area of this line as a function of the

cell temperature (green curve in Figure 4C). The decomposition of nitrate anions is complete above 473 K. The decomposition onset of the AlMo$_6$ Anderson-type species is marked by the broadening of the line located around 910−950 cm^{-1} (see Figure 4B) and by the intensity decrease of both 210 (not followed in Figure 4C) and 565 cm^{-1} lines (pink curve in Figure 4C). It occurs around 408 K (marked with a dashed line), a temperature corresponding to the decomposition of the reference ammonium Anderson salt. Concomitantly to the vanishing of the lines characterizing the Anderson-type heteropolyanion, a strong broadening and an intensity increase of the line area between 300 and 425 cm^{-1} occur (black curve in Figure 4C). Considering that the latter line is characteristic of the wagging mode of the terminal Mo=O$_t$ bonds,[39] the concomitant intensity variation of both lines at 350 (black curve) and 565 cm^{-1} (pink curve) is the clear evidence that the decomposition of the Anderson-type heteropolyanion occurs in this temperature range and is complete around 448 K. The further increase of the cell temperature above 448 K gives rise to the broadening of the main line at 955 cm^{-1}.

At 723 K, the well-defined lines characteristic of NiMoO$_4$ crystallites[56] or of MoO$_3$[35] are not observed in the Raman spectrum of the dehydrated-calc-NiMo catalyst, which confirms the good dispersion of the oxomolybdate entities on the alumina support. This spectrum (Figure 4B) is characteristic of the dehydrated-calc-NiMo precursor with surface polymeric dehydrated entities as already observed.[43] All these results suggest that, upon heating, these polymeric oxomolybdate entities are mainly formed by the decomposition of AlMo$_6$ species followed by grafting on the support through a dehydration process.

ii. XAS Characterization. The changes of Mo and Ni K edge XANES spectra observed upon *in situ* calcination are presented in Figures 5A and 5B, respectively.

Mo K Edge Characterization. As shown in Figure 5A, an increase of the intensity of the pre-edge structure (inset in the figure) first occurs (376−516 K) together with the merge of resonances located at 20041 and 20054 eV characterizing the
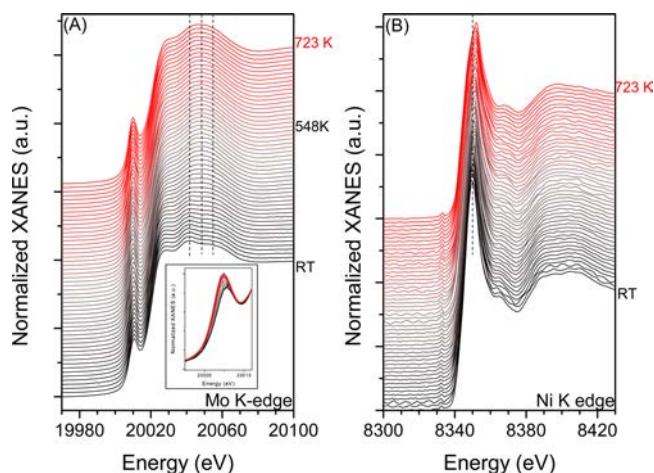
Figure 5. *In situ* monitoring of the calcination of the dried-NiMo catalyst by Quick-XAS at the Mo K edge (A) and at the Ni K edge (B). The inset is a zoom of the pre-edge region for the Mo K edge XAS spectra.

dried-NiMo catalyst into a featureless resonance centered at ~20049 eV. The first coordination shell of Mo at 548 K is described by 4.5 ± 0.6 oxygen atoms at the distance of 1.74 (0.01) Å from the Mo absorbing atom (Table 3, fit G). This result is in good agreement with the interpretation of LRS and XANES results previously discussed for the dehydrated-calc-NiMo catalyst in section 3.a.ii.

Table 3. Fit EXAFS Parameters of the Dehydrated-calc-NiMo Sample at 548 K and of the Nickel Intermediate Species Identified by MCR-ALS

backscatterer	N	R (Å)	σ^2 (Å^2) × 10^3	R-factor	χ^2_ν
		Dehydrated-calc-NiMo, Fit G (548 K)			
O	4.5 ± 0.6	1.74 ± 0.01	6.4 ± 1.3	0.0029	11
Mo K edge, $\Delta k = 4.5-12.0$ Å^{-1}, $S_0^2 = 0.8$, $E_0 = 20020.66$ eV, enot = -5.01 eV					
		Component 1, Fit H			
O	4.4 ± 1.6	2.01 ± 0.03			
Al	1.9 ± 1.6	2.85 ± 0.05	6.7 ± 4.4	0.0016	50
Ni	1.9 ± 1.2	2.85 ± 0.05	42.9 ± 3.3		
Ni K edge, $\Delta k = 4.1-10$ Å^{-1}, $S_0^2 = 0.8$, $E_0 = 8348$ eV, enot = -3.23 eV					
		Component 2, Fit I			
O	5.8 ± 1.5	2.04 ± 0.01	9.5 ± 3.2	0.0166	69
Ni K edge, $\Delta k = 4.3-10.0$ Å^{-1}, $S_0^2 = 0.8$, $E_0 = 8348$ eV, enot = -3.40 eV					

Ni K Edge Characterization. At the Ni K edge, slight modifications of the shape of the XANES spectra (Figure 5B) occur affecting essentially the intensity and energy position of the white line, as already discussed in section 3.a.iii. After the nitrate decomposition, it has been observed that the maximum of the white line of the Ni K edge spectrum is shifted to higher energy (Figure 5B). The shift reaches about +2 eV at 723 K. The analysis by MCR-ALS of the nickel speciation occurring during the calcination process is not straightforward due to the presence of a mixture of phases after impregnation, i.e., NiAl-based LDH phase and nickel $Ni(H_2O)_x(OH)_y$, each suffering a different phase transformation upon calcination. The identification of the species formed at the end of the calcination was achieved using a multiple set data analysis by MCR-ALS, called data augmentation method,[57,58] considering the whole treatment suffered by the catalyst, i.e., calcination followed by

sulfidation without intermediate contact with air moisture. Because the relative concentrations of oxidic species varied differently in the calcination and in the sulfidation, the addition of the data recorded upon both processes allowed us to isolate two oxidic components as products of calcination and starting phases of sulfidation treatment. The components so-extracted by MCR-ALS of the augmented data set are characterized by the XANES spectra displayed in Figure 6A. The comparison of the XANES spectrum related to the first component with the spectrum of a bulk $NiAl_2O_4$ reference shows that all spectral features are well in phase (Figure 6B). In particular, the characteristic white lines shifted at higher energy by about +2 eV compared to the dried-NiMo catalyst are well aligned in position. This suggests that the first species isolated by MCR-ALS is a species presenting a local order very similar to the one encountered in nickel aluminate in which the Ni ions can occupy the octahedral and tetrahedral surface sites of the support as nickel aluminate always displays a partially inversed spinel structure.[59] As a matter of fact, the EXAFS spectrum associated with this first component can be satisfactorily simulated considering the next nearest nickel and aluminum neighbors encountered in nickel aluminate.[60] Fitting in R space can be found in Figure S7A (Table 3, fit H).

The XANES spectrum of the second nickel oxidic component isolated by MCR-ALS (Figure 6A) displays a pre-edge peak of small intensity and a general shape characteristic of octahedral nickel species with an intense white line located at lower energy than the white line of the first component. Actually, as shown in Figure 6C, the white line and general shape of this second component are well in phase with the spectrum of the NiO bulk reference. The Fourier transform of the EXAFS spectrum of the second component displayed in Figure S7B presents a first intense contribution related to the first coordination shell (Table 3, fit I) with fitted coordination number in agreement with the octahedral symmetry suggested by the XANES shape. The assignment to a peculiar path is difficult for the broad contribution appearing at a distance longer than 2.5 Å on the FT (not phase corrected) of the second MCR-ALS component. Nevertheless, it is noteworthy that the fitting of the dehydrated-calc-NiMo catalyst (fit E, Table 2) has previously evidenced as second neighbors a Ni−Al contribution at 2.89 (0.04) Å in good agreement with the structure of $NiAl_2O_4$[55] and a Ni−Ni contribution located at 3.01 Å which could be satisfactorily explained with the Ni−Ni distance at 2.98 Å found in NiO.[61] The in-depth analysis of the transformation suffered by the nickel upon *in situ* calcination by MCR-ALS analysis, together with the fit reported for the dehydrated-calc-NiMo catalyst, allows us to propose that the calcination of the dried-NiMo catalyst leads before air moisture exposure to the formation of the nickel aluminate-type species and of octahedral Ni oxidic condensed species. By LCF using the two components determined by MCR-ALS analysis, it can be estimated that the composition of the dehydrated-calc-NiMo catalyst is made of ~34% $NiAl_2O_4$-type and ~66% Ni oxidic species (octahedral Ni) (Figure S8 and Table S1).

Finally, considering the reported speciation of the dehydrated-calc-NiMo catalyst, a multicombinatorial LCF of the RT XANES spectrum of the calc-NiMo sample has been carried out using the spectra of both components determined by MCR-ALS analysis of the data set recorded upon *in situ* calcination and the RT spectrum of the NiAl-based LDH phase, already used for simulating the RT dried-NiMo catalyst. According to the values reported for the R_F-factor and for the
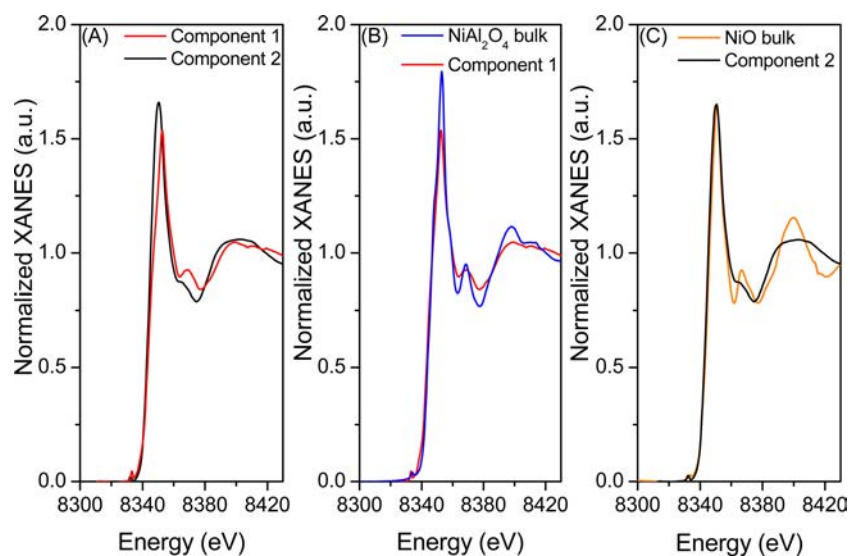
Figure 6. Ni K edge XANES spectra determined by MCR-ALS as components involved during the calcination of the dried-NiMo catalyst (A), the first component determined by MCR-ALS compared to the NiAl$_2$O$_4$ bulk reference (B), and the second component determined by MCR-ALS compared to the NiO bulk reference (C).

reduced χ_ν^2 quality factor for the different combinations, the best LCF is obtained considering ~62% of NiAl-based LDH phase and ~38% of the octahedral Ni oxidic species (second MCR-ALS component) (Figure S9 and Table S1). This fully confirms the recovery of the NiAl-based LDH phase upon air moisture contact of the dehydrated-calc-NiMo catalyst.

c. Characterization of the Different Sulfide Catalysts. The sulfidation was carried out *in situ* at the SAMBA beamline. The characterization presented below was obtained at the end of the heating ramp at 673 K under H$_2$S/H$_2$ atmosphere. It corresponds to the first 5 min under isothermal treatment.

Mo K Edge Characterization. Figure 7 displays for the three sulfide samples the Mo K edge XANES and corresponding FTs in comparison with a bulk MoS$_2$ reference phase. The corresponding EXAFS signals are presented in Figure S10. The spectra of the final molybdenum phases present in the
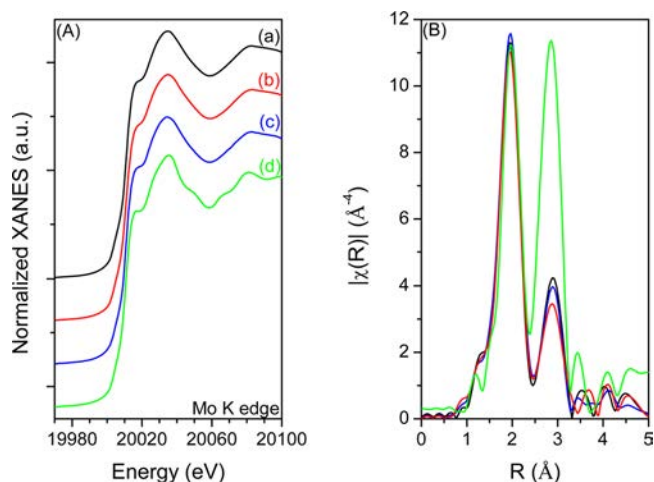

Figure 7. (A) Mo K edge XANES and (B) FT modulus data recorded at the end of the heating ramp of the sulfidation (673 K) for the three catalysts: (a) dried-sulf-NiMo (black); (b) dehydrated-calc-sulf-NiMo (red); (c) calc-sulf-NiMo (blue). (d) MoS$_2$ reference data (RT) are reported for comparison purpose (green, the corresponding FT is multiplied by a factor 0.6 for the sake of clarity).

rising edge a very similar XANES spectrum to the one of the MoS$_2$ phase (Figure 7A) with a well-resolved shoulder around 20017 eV. The smoothing of the structures above the main resonance located at 20035 eV compared to the bulk MoS$_2$ phase arises from the formation of nanocrystalline MoS$_2$ slabs. The EXAFS oscillations are in phase with the ones of the MoS$_2$ reference (Figure S10). The contribution located around 2.93 Å on the FTs of the EXAFS signals recorded at the end of the sulfidation for the three catalysts (Figure 7B) is characteristic of the Mo–Mo distance in MoS$_2$ (3.17 Å). The results of the best fits are presented in Table 4 (fits J–L) (Figure S11A). The fittings have been performed with a constant number of sulfur atoms (equal to 6) for the first coordination shell since, as verified by Plazenet et al.,[62] the coordination number for the first coordination shell of nano-MoS$_2$ does not depend on the nanometric size of the slabs. The higher Debye–Waller factors found for the catalysts in comparison with the MoS$_2$ bulk reference (Table 4, M) are related to the temperature of the measurement (673 K). The coordination numbers found for the Mo–Mo contribution are substantially smaller than those of bulk MoS$_2$: this feature is typical of the formation of nanocrystalline MoS$_2$ slabs as discussed in the literature.[39] This is in agreement with the TEM characterization shown in Figure S12 for the dried-sulf-NiMo and calc-sulf-NiMo samples. Although the variation of the Mo–Mo coordination numbers for the three catalysts is within the error bars, in agreement with the evolution of the intensity of the Mo–Mo contribution on the FTs, we may consider that this parameter is directly linked to the hydration state of the catalyst that influences the nature of the oxomolybdate surface species. The statistical analysis of the TEM pictures evidenced a slight decrease of the size of the MoS$_2$ slab for the calc-NiMo catalyst compared to the dried-NiMo one (Figure S12). As pointed out by the lowest Fourier transformed Mo–Mo contribution, a more drastic effect is observed for the dehydrated-calc-sulf-NiMo catalyst.

Ni K Edge Characterization. Figure 8 displays for the three sulfide samples the Ni K edge XANES and corresponding FTs in comparison with a bulk Ni$_3$S$_2$ reference phase. The XANES spectra are characterized by a broad resonance characteristic of sulfide nickel species like Ni$_3$S$_2$ presented herein (Figure 8A).

Table 4. Mo K Edge Fit EXAFS Parameters of the Sulfide Samples (673 K). Fit parameters of the MoS2 reference (RT) are also reported.[a]

backscatterer	N	R (Å)	σ^2 (Å^2) $\times 10^3$	R-factor	χ^2_ν
		Dried-sulf-NiMo, Fit J (673 K)			
S	6	2.41 ± 0.01	5.5 ± 0.54	0.0082	249
Mo	2.8 ± 0.5	3.18 ± 0.01			
		Dehydrated-calc-sulf-NiMo, Fit K (673 K)			
S	6	2.41 ± 0.01	5.7 ± 0.5	0.0089	408
Mo	2.5 ± 0.6	3.17 ± 0.01			
		Calc-sulf-NiMo, Fit L (673 K)			
S	6	2.41 ± 0.01	5.1 ± 0.5	0.0081	86
Mo	2.5 ± 0.5	3.17 ± 0.01			
		MoS$_2$, Fit M (RT)			
S	6	2.41 ± 0.01	2.1 ± 0.7	0.0113	1004
Mo	6	3.17 ± 0.01	1.7 ± 0.4		

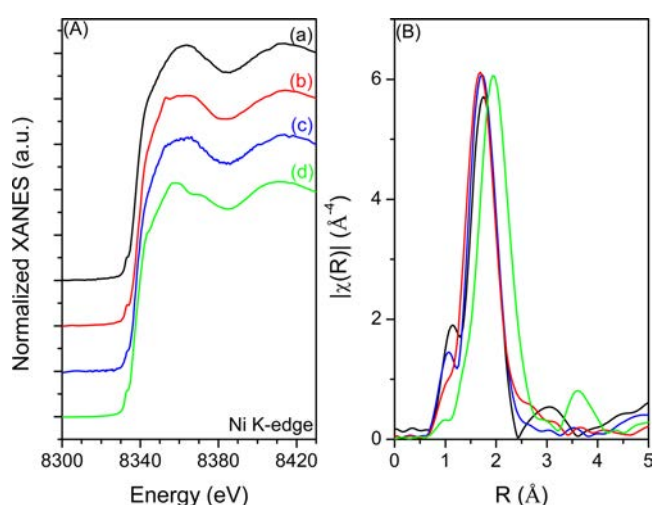[a]Δk = 3−12.5 Å−1, S02 = 0.8, E0 = 20010.50 eV, enot = 2.21 eV.

Figure 8. (A) Ni K edge XANES and (B) FT modulus data recorded at the end of the heating ramp of the sulfidation (673 K) for the three catalysts: (a) dried-sulf-NiMo (black); (b) dehydrated-calc-sulf-NiMo (red); (c) calc-sulf-NiMo (blue). (d) Ni$_3$S$_2$ reference data (RT) are reported for comparison purpose (green, the corresponding FT data is multiplied by a factor 0.6 for sake of clarity).

Nevertheless the XANES spectra of catalysts are super-imposable neither to the one of the Ni$_3$S$_2$ reference nor to the spectra of NiS and NiS$_2$ reported in the literature.[63,64] Actually the shape of the XANES spectra of the sulfide catalysts is very similar to the one published by Hamabe et al.[65] for a homemade sulfide NiMo/Al$_2$O$_3$ catalyst (Ni/Mo = 0.2), which was identified as representative of the active NiMoS phase[66] by the analysis of RT EXAFS data in an extended k-range. It is nevertheless important to note that, as for the spectrum reported by Hamabe et al., the XANES spectra reported for the calcined sulfided catalysts (calc-sulf-NiMo and dehydrated-calc-sulf-NiMo) display at 8353 eV a small bump that we ascribe as a reminiscence of the white line characteristic of the NiAl$_2$O$_4$-type species. Considering that the dried-sulf-NiMo catalyst is representative of a fully sulfided species, its XANES spectrum is used with the XANES spectrum determined by MCR-ALS for the NiAl$_2$O$_4$-type species to fit the XANES spectra of both calc-sulf-NiMo and dehydrated-calc-sulf-NiMo catalysts. The LC fitting procedure gives a quite similar proportion of NiAl$_2$O$_4$-type species remaining at this early stage of the sulfidation equal to about 6 to 10%. The main contribution of the Fourier

transform of the three sulfide samples is located at shorter distance than the one of Ni$_3$S$_2$ reference (Figure 8B). As presented in Table 5 (fit N), the fit of this latter contribution

Table 5. Ni K Edge Fit EXAFS Parameters of the Sulfide Samples (673 K). Fit parameters of the Ni3S2 reference (RT) are also reported.[a]

backscatterer	N	R (Å)	σ^2 (Å^2) $\times 10^3$	R-factor	χ^2_ν
		Ni$_3$S$_2$, Fit N (RT)			
S	4	2.27 ± 0.01	8.6 ± 1.9	0.0127	163
Ni	4	2.51 ± 0.01	10.1 ± 1.9		
		Dried-sulf-NiMo, Fit O (673 K)			
S	3.8 ± 0.8	2.21 ± 0.01	9.7 ± 3.4	0.0106	220
		Dehydrated-calc-sulf-NiMo, Fit P (673 K)			
S	3.1 ± 0.8	2.21 ± 0.01	7.4 ± 4.0	0.0197	553
		Calc-sulf-NiMo, Fit Q (673 K)			
S	3.4 ± 0.7	2.21 ± 0.01	8.1 ± 3.1	0.0171	61

Δk = 3−9.5 Å−1, S02 = 0.8, E0 = 8336.72 eV, enot = 0.85 eV.

[a]Δk = 3−9.5 Å−1, S02 = 0.8, E0 = 8336.72 eV, enot = 0.85 eV.

requires Ni−S and Ni−Ni distances at 2.27 (0.01) Å and 2.51 (0.01) Å. For the three catalysts, the first main FT contribution is satisfactorily reproduced with a lone sulfur coordination shell at 2.21 (0.01) Å (Table 5 and Figure S11B). This Ni−S distance is well in line with the distance found by Koizumi et al. for the active NiMoS phase.[66] Then, although the EXAFS acquisition at high temperature and the limited available k-range do not allow us to identify herein in the experimental data the Ni−Mo contribution characteristic of the NiMoS phase around 2.73−2.76 Å determined in other works,[67,68] our Ni K edge XAS results strongly suggest the formation of NiMoS active species.

4. DISCUSSION

The in-depth study of the as-prepared dried-NiMo sample by Raman and X-ray absorption spectroscopies evidences that no interaction between nickel and molybdenum atoms exists at the oxide state. The dried-NiMo catalyst is mainly composed of AlMo$_6$ species and of Ni oxo/hydroxo and NiAl-based LDH species. We observe as well that calcination of the dried-NiMo sample does not lead to the formation of a mixed NiMo oxidic phase since no interaction between both metallic centers has been observed at short distance. The modification occurring at

any stage of the catalyst genesis has been then analyzed separately in the following.

At the early stages of the catalyst preparation, the formation of AlMo$_6$ based species has been already discussed by several groups. It has been shown that it involved quantitative reactions of Mo ions with lixiviated aluminum species,[3,69,70] the reaction occurring in the solution in the pores during the maturation step of the preparation of the catalyst in wet atmosphere as demonstrated by Carrier et al.[70] and Le Bihan et al.[3] The unambiguous evidence (by LRS and XAS) of the formation of the Anderson-type AlMo$_6$ species reveals that, in the chemical peroxo route used herein, similar dissolution of the support takes place during this stage. It is followed by recombination of the aluminate species with the oxomolybdate species coming from the decomposition of peroxomolybdate species present in the solution. Interestingly, although Ni or Mo building blocks can react with lixiviated Al^{3+} species, with the preparation method used in this work, no evidence of a reaction between both metals leading to the formation of the Anderson 6-molybdonickelate entity (NiMo$_6$O$_{24}$H$_6$)$^{3-}$ or the dimeric species (Ni$_2$Mo$_{10}$O$_{38}$H$_4$)$^{6-}$ has been observed by XAS and Raman.[71] This result is in line with those reported by Lamonier et al.[71] showing that the maturation and drying steps of NiMo catalysts prepared by impregnation of alumina with a solution of ammonium heptamolybdate and nickel nitrate still form a well-dispersed AlMo$_6$ phase.

EXAFS results evidenced that these AlMo$_6$ species are yet in interaction with the support after the drying step. Upon calcination and before contact with air moisture, transformation of the Anderson-type AlMo$_6$ species occurs, mainly leading to distorted tetrahedral oxomolybdenum units which are isolated and/or inserted in polyoxomolybdate entities both being in interaction with the support. Upon calcination with a 5 K/min ramp and further air moisture contact, EXAFS and Raman spectroscopies show that the Anderson-type AlMo$_6$ species are partly recovered, with some nonclearly identified intermediates of rehydration. Such a rehydration phenomenon has been already observed and discussed,[3] but due to the high degree of rehydration a total recovery of the Anderson entities was evidenced.

Dealing with the nickel species formed after incipient wetness impregnation, the formation of NiAl-based LDH reported herein can be related to the work observed by d'Espinose de la Caillerie et al.[72] These authors showed that, under neutral and basic conditions (pH > 7), bulk NiAl-based LDH phase can be formed from the dissolution of aluminum ions from a γ-alumina support and reprecipitation with the nickel ions in solution during the impregnation stage. Besides, the possible formation of Al-containing hydrotalcite phase on the surface of alumina was also reported by de Bokx et al.[73] The amount of the Ni (67% as determined by XANES LCF) that has not reacted to form the aforementioned LDH is spread at the surface as Ni(H$_2$O)$_x$(OH)$_y$ species.

Upon calcination/dehydration, the formation of a mixture of amorphous nickel aluminate and amorphous octahedral oxidic Ni species has been evidenced. As reported in the literature,[5] for low loaded NiO/γAl$_2$O$_3$ catalysts, amorphous diluted Ni–Al spinel and amorphous NiO overlayer have been observed during calcination studies. Then we propose to relate the amorphous octahedral oxidic Ni species corresponding to the second MCR-ALS component to the formation of the amorphous overlayer of NiO. It is noteworthy that the presence of the aluminate-like phase can be also related to

the formation of the surface NiAl-LDH phase at the early stage of catalyst preparation.[74] Recently, a description of the mechanisms underlying the transformation of LDH phases into bulk nanoaluminate spinel phases at moderate temperatures was reported by Carvalho et al.[25] In the case of the thermal decomposition under static air atmosphere of ZnAl-LDH phase containing Cl as ions in the interlayer space, the formation of ZnO and ZnAl$_2$O$_4$ nanophases was observed at 723 K. The proportion of divalent oxide and spinel-like oxide was evidenced as being strongly dependent on the heating ramp used for the calcination treatment. For a heating rate of 5 K/min, the spinel-like oxide is dominant with about 80%. The opposite composition, i.e., 20% of spinel-like oxide phase, can be achieved with a faster heating rate (10 K/min). It is noteworthy that the as-prepared spinel-like phase remains amorphous with respect to its detection by X-ray diffraction (XRD) evidencing its nanometer size. This finding explains that its formation was only revealed at high temperature by XRD and only speculated at moderate temperatures ($T < 723$ K) as surface alumina spinel species from local order technique results such as FTIR (Fourier transform infrared spectroscopy) or EXAFS.[73−75] Interestingly, the in-depth Quick-XAS study of transformation of LDH-like phase into spinel-like species upon thermal treatment[25] suggests that the percentage of formed aluminate spinel phases during catalyst pretreatment could be controlled by the heating rate of calcination. Herein the treatment condition leads for the dehydrated-calc-NiMo catalyst to ~34% of aluminate species and ~66% of an amorphous nickel oxide overlayer, proportions that are close to the Ni speciation in the dried-NiMo catalyst.

The *ex situ* calcination followed by transfer in air moisture clearly evidences a recovery of the NiAl-based LDH phase characterizing the dried-NiMo catalyst with ~38% of NiAl-LDH based phase and ~62% of octahedral amorphous NiO species. These findings are related to the rehydration of the species upon exposure to air moisture already noted for the Mo species.[3] For the Ni species, this behavior is due to the well-known "memory effect" of LDH based compounds.[76,77] Indeed, the recovery of the original layered structure of LDH, after contact with water of the products obtained upon LDH thermal decomposition at moderate temperature (typically up to 673−723 K), is observed. Such a behavior starts to be studied for catalytic applications since it can be advantageously used for catalyst regeneration and/or structuration.[78,79] The observed recovery of LDH phase and AlMo$_6$ species emphasizes the essential aspect of the surface oxidic species formation that must be carefully controlled in order to tailor the catalytic performances.

Upon sulfidation, whatever the catalyst (i.e., dried-sulf-NiMo, calc-sulf-NiMo, dehydrated-calc-sulf-NiMo), the formation of well-dispersed MoS$_2$ slabs was evidenced. Nevertheless a small dependence of their morphology with the oxidic precursor treatment was observed. It can be related to the nature of the supported oxomolybdate entities. Regarding the promoter, the transformation toward aluminate species of the oxidic species upon calcination appears as a leveling step of the sulfidation since aluminate spinel-like species are often difficult to reduce or sulfide. As a matter of fact, 10% of the aluminate species for the dehydrated-calc-NiMo catalyst remains after the sulfidation. Nevertheless their relative proportion in the sulfide catalyst is smaller than in the oxidic form, suggesting that part of this aluminate species is well-dispersed at the surface of the support. Despite the contact with air moisture after calcination which

favors the regeneration of NiAl-based LDH species, differences between the sulfidation state of the dried-NiMo catalyst and calc-NiMo catalyst at the early stage of sulfidation have been also pointed out. Such a difference could result from differences in morphology and/or crystallite size of the regenerated LDH phase compared to the parent one.[80] The EXAFS data for the sulfide nickel species were reported at 673 K; at this high temperature, the inherent damping of the EXAFS oscillations does not allow us to evidence the presence of Ni−Mo bonds. However, the reported results strongly suggest the formation of the NiMoS active species. The in-depth analysis of the concomitant evolution of the Mo and Ni species measured during catalyst sulfidation using time-resolved XAS/Raman spectroscopies, presented in a forthcoming paper, will allow us to understand the genesis of the HDS active phases and establish a relationship with the surface species of the oxidic precursors.

5. CONCLUSION

The pretreatment of the oxide catalyst precursor is of paramount importance for the speciation of the metallic centers that governs further the speciation of the sulfide catalysts. The formation of the $AlMo_6$ entities, well established with the AHM starting precursor, is also observed with the peroxo route involving MoO_3 together with the formation of layered double hydroxide phase involving Ni and Al atoms. Our results do not report any evidence of the formation of mixed NiMo heteropolyanions, and both metals are not in interaction on the oxide catalyst precursor whatever the treatment (drying/calcination/rehydration). The calcination treatment seems detrimental toward the Ni promoter as we clearly evidenced that bulk and/or surface LDH phase formed at the early stage of the preparation will be partly transformed into spinel aluminate nickel species. However, we have shown that the hydration conditions strongly govern the Mo and Ni speciation after calcination. In particular, a partial regeneration of $AlMo_6$ entities and NiAl-LDH species is obtained for the calcined catalyst not preserved from air moisture. The dehydrated state of catalyst before sulfidation and, at lower level, the calcination are responsible for incomplete sulfidation of the nickel species. Fortunately, despite an important amount of NiAl-based species before starting the sulfidation (about 35% of LDH or $NiAl_2O_4$-based species depending on the treatment), most of them can be sulfided, suggesting that it deals with well-dispersed surface nickel aluminate species.

ASSOCIATED CONTENT

Ⓢ Supporting Information

The Supporting Information is available free of charge on the ACS Publications website at DOI: 10.1021/acs.jpcc.5b06219.

> LCF results of XANES spectra, Raman spectra, EXAFS data and fittings, and TEM images (PDF)

AUTHOR INFORMATION

Corresponding Authors
*E-mail: amelie.rochet@lnls.br. Phone: 00 55 19 35 17 51 80.
*E-mail: virginie.moizan@ifp.fr. Phone: 00 33 4 37 70 23 59.

Present Address
§Laboratório Nacional de Luz Síncrotron, CEP 13083-970, Caixa Postal 6192, Campinas, São Paulo, Brazil. Phone: 00 55 19 35 17 51 80. E-mail: amelie.rochet@lnls.br.

Notes
The authors declare no competing financial interest.

ABBREVIATIONS

XAS, X-ray absorption spectroscopy; EXAFS, extended X-ray absorption fine structure; XANES, X-ray absorption near edge structure; Quick-XAS, Quick-EXAFS; LRS, laser Raman spectroscopy; FT, Fourier transform; RT, room temperature; LCF, linear combination fitting; TEM, transmission electron microscopy; XRD, X-ray diffraction; FTIR, Fourier transform infrared spectroscopy; AHM, ammonium heptamolybdate

REFERENCES

(1) Song, C. S. An Overview of New Approaches to Deep Desulfurization for Ultra-Clean Gasoline, Diesel Fuel and Jet Fuel. *Catal. Today* **2003**, *86*, 211−263.

(2) Topsøe, H.; Candia, R.; Topsøe, N.-Y.; Clausen, B. S.; Topsøe, H. On The State of the Co-Mo-S Model. *Bull. Soc. Chim. Belg.* **1984**, *93*, 783−806.

(3) Le Bihan, L.; Blanchard, P.; Fournier, M.; Grimblot, J.; Payen, E. Raman Spectroscopic Evidence for the Existence of 6-molybdoaluminate Entities on an Mo/Al_2O_3 Oxidic Precursor. *J. Chem. Soc., Faraday Trans.* **1998**, *94*, 937−940.

(4) Bolt, P. H.; Habraken, F. H. P. M.; Geus, J. W. J. Formation of Nickel, Cobalt, Copper, and Iron Aluminates from α- and γ-Alumina-Supported Oxides: A Comparative Study. *J. Solid State Chem.* **1998**, *135*, 59−69.

(5) Salagre, P.; Fierro, J. L. G.; Medina, F.; Sueiras, J. E. Characterization of Nickel Species on Several Gamma-Alumina Supported Nickel Samples. *J. Mol. Catal. A: Chem.* **1996**, *106*, 125−134.

(6) Blanchard, P.; Lamonier, C.; Griboval, A.; Payen, E. New Insight in the Preparation of Alumina Supported Hydrotreatment Oxidic Precursors: A Molecular Approach. *Appl. Catal., A* **2007**, *322*, 33−45.

(7) Bergwerff, J. A.; Jansen, M.; Leliveld, B. G.; Visser, T.; de Jong, K. P.; Weckhuysen, B. M. Influence of the Preparation Method on the Hydrotreating Activity of MoS_2/Al_2O_3 Extrudates: A Raman Microspectroscopy Study on the Genesis of the Active Phase. *J. Catal.* **2006**, *243*, 292−302.

(8) Chen, W.; Maugé, F.; van Gestel, J.; Nie, H.; Li, D.; Long, X. Effect of Modification of the Alumina Acidity on the Properties of Supported Mo and CoMo Sulfide Catalysts. *J. Catal.* **2013**, *304*, 47−62.

(9) Carrier, X.; Lambert, J. F.; Che, M. Ligand-Promoted Alumina Dissolution in the Preparation of $MoO_x/\gamma-Al_2O_3$ Catalysts: Evidence for the Formation and Deposition of an Anderson-type Alumino Heteropolymolybdate. *J. Am. Chem. Soc.* **1997**, *119*, 10137−10146.

(10) Guevara-Lara, A.; Bacaud, R.; Vrinat, M. Highly Active NiMo/TiO_2 Al_2O_3 Catalysts: Influence of the Preparation and the Activation Conditions on the Catalytic Activity. *Appl. Catal., A* **2007**, *328*, 99−108.

(11) Payen, E.; Kasztelan, S.; Grimblot, J. In Situ Laser Raman Spectroscopy of the Sulphiding of $WO_3(MoO_3)/\gamma−Al_2O_3$ catalysts. *J. Mol. Struct.* **1988**, *174*, 71−76.

(12) Knözinger, H.; Mestl, G. Laser Raman Spectroscopy − a Powerful Tool for In Situ Studies of Catalytic Materials. *Top. Catal.* **1999**, *8*, 45−55.

(13) Bañares, M. A. Operando Spectroscopy: the Knowledge Bridge to Assessing Structure-Performance Relationships in Catalyst Nanoparticles. *Adv. Mater.* **2011**, *23*, 5293−5301.

(14) Tsigdinos, G. A.; Chen, H. Y.; Streusand, B. J. Molybdate Solutions for Catalyst Preparation. Stability, Adsorption Properties,

and Characterization. *Ind. Eng. Chem. Prod. Res. Dev.* **1981**, *20*, 619−623.

(15) Payen, E.; Guillaume, D.; Lamonier, C.; Marchand, K. Method of Preparing at least one Cobalt and/or Nickel Salt of at least one Anderson's Heteropolyanion Combining Molybdenum and Cobalt or Nickel in its Structure; EP 1892038 A1February 27, 2008.

(16) Moreau, J.; Delpoux, O.; Devers, E.; Digne, M.; Loridant, S. Decamolybdocobaltate Heteropolyanions in Aqueous Solutions: Chemistry Driving their Formation and Domains of Stability. *J. Phys. Chem. A* **2012**, *116*, 263−270.

(17) Moreau, J.; Delpoux, O.; Devers, E.; Digne, M.; Loridant, S. Impregnation of Decamolybdocobaltate Heteropolyanions over γ-Alumina: Detailed Description of the Physico-Chemical Phenomena. *Langmuir* **2013**, *29*, 207−215.

(18) La Fontaine, C.; Barthe, L.; Rochet, A.; Briois, V. X-ray Absorption Spectroscopy and Heterogeneous Catalysis: Performances at the SOLEIL's SAMBA Beamline. *Catal. Today* **2013**, *205*, 148−158.

(19) Briois, V.; Fonda, E.; Belin, S.; Barthe, L.; La Fontaine, C.; Langlois, F.; Ribbens, M.; Villain, F. SAMBA: The 4−40 keV X-ray Absorption Spectroscopy Beamline at SOLEIL. *UVX 2010 - 10e Colloque sur les Sources Cohérentes et Incohérentes UV, VUV et X: Applications et Développements Récents* **2010**, 41−47.

(20) Fonda, E.; Rochet, A.; Ribbens, M.; Barthe, L.; Belin, S.; Briois, V. The SAMBA Quick-EXAFS Monochromator: XAS with Edge Jumping. *J. Synchrotron Radiat.* **2012**, *19*, 417−424.

(21) Ravel, B.; Newville, M. Athena, Artemis, Hephaestus: Data Analysis for X-Ray Absorption Spectroscopy Using Ifeffit. *J. Synchrotron Radiat.* **2005**, *12*, 537−541.

(22) Newville, M. IFEFFIT: Interactive XAFS Analysis and FEFF Fitting. *J. Synchrotron Radiat.* **2001**, *8*, 322−324.

(23) Conti, P.; Zamponi, S.; Giorgetti, M.; Berrettoni, M.; Smyrl, W. H. Multivariate Curve Resolution Analysis for Interpretation of Dynamic Cu K-Edge X-ray Absorption Spectroscopy Spectra for a Cu Doped V$_2$O$_5$ Lithium Battery. *Anal. Chem.* **2010**, *82*, 3629−3635.

(24) Nunes, C. A.; Resende, E. C.; Aes, I. G. R.; Anastacio, A. S.; Guerreiro, M. C. In-situ Monitoring of the Structure of a Goethite-Based Catalyst During Methane Oxidation by X-ray Absorption Near-Edge Structure (XANES) Spectroscopy Assisted by Chemometric Methods. *Appl. Spectrosc.* **2011**, *65*, 692−697.

(25) Carvalho, H. W. P.; Pulcinelli, S. H.; Santilli, C. V.; Leroux, F.; Meneau, F.; Briois, V. XAS/WAXS Time-Resolved Phase Speciation of Chlorine LDH Thermal Transformation: Emerging Roles of Isovalent Metal Substitution. *Chem. Mater.* **2013**, *25*, 2855−2867.

(26) Cassinelli, W. H.; Martins, L.; Passos, A. R.; Pulcinelli, S. H.; Santilli, C. V.; Rochet, A.; Briois, V. Multivariate Curve Resolution Analysis Applied to Time-resolved Synchrotron X-ray Absorption Spectroscopy Monitoring of the Activation of Copper Alumina Catalyst. *Catal. Today* **2014**, *229*, 114−122.

(27) Staniuk, M.; Hirsch, O.; Kränzlin, N.; Böhlen, R.; van Beek, W.; Abdala, P. M.; Koziej, D. Puzzling Mechanism behind a Simple Synthesis of Cobalt and Cobalt Oxide Nanoparticles: In Situ Synchrotron X-ray Absorption and Diffraction Studies. *Chem. Mater.* **2014**, *26*, 2086−2094.

(28) Voronov, A.; Urakawa, A.; Beek, W. v.; Tsakoumis, N. E.; Emerich, H.; Rønning, M. Multivariate Curve Resolution Applied to in situ X-ray Absorption Spectroscopy Data: An Efficient Tool for Data Processing and Analysis. *Anal. Chim. Acta* **2014**, *840*, 20−27.

(29) Hong, J.; Marceau, E.; Khodakov, A. Y.; Gaberová, L.; Griboval-Constant, A.; Girardon, J.-S.; La Fontaine, C.; Briois, V. Speciation of Ruthenium as a Reduction Promoter of Silica-Supported Co Catalysts: A Time-Resolved In Situ XAS Investigation. *ACS Catal.* **2015**, *5*, 1273−1282.

(30) Jaumot, J.; Gargallo, R.; de Juan, A.; Tauler, R. A Graphical User-friendly Interface for MCR-ALS: a new Tool for Multivariate Curve Resolution in MATLAB. *Chemom. Intell. Lab. Syst.* **2005**, *76*, 101−110.

(31) Prevot, V.; Briois, V.; Cellier, J.; Forano, C.; Leroux, F. An In-situ Investigation of LDH−Acetate Prepared in Polyol, under

Moderate Thermal Treatment. *J. Phys. Chem. Solids* **2008**, *69*, 1091−1094.

(32) Alía, J. M. Raman Spectroscopic Studies of Ion−Ion Interactions in Aqueous and Nonaqueous Electrolyte Solutions. In *Handbook of Raman Spectroscopy*; Lewis, I. R., Edwards, H. G. M., Eds.; Marcel Dekker, Inc.: New York, 2001; pp 617−682.

(33) Taylor, R. C.; Cross, P. C. Raman Spectra of Hydrogen Peroxide in Condensed Phases. I. The Spectra of the Pure Liquid and its Aqueous Solutions. *J. Chem. Phys.* **1956**, *24*, 41−44.

(34) Arab, M.; Bougeard, D.; Aubry, J. M.; Marko, J.; Paul, J. F.; Payen, E. Structure and Raman Spectra of Transient Species in the Catalytic Disproportionation of Hydrogen Peroxide by Molybdate Ions. *J. Raman Spectrosc.* **2002**, *33*, 390−396.

(35) Tian, H.; Roberts, C. A.; Wachs, I. E. Molecular Structural Determination of Molybdenum in Different Environments: Aqueous Solutions, Bulk Mixed Oxides, and Supported MoO$_3$ Catalysts. *J. Phys. Chem. C* **2010**, *114*, 14110−14120.

(36) Kalampounias, A. G.; Tsilomelekis, G.; Berg, R. W.; Boghosian, S. Molybdenum(VI) Oxosulfato Complexes in MoO$_3$-K$_2$S$_2$O$_7$-K$_2$SO$_4$ Molten Mixtures: Stoichiometry, Vibrational Properties, and Molecular Structures. *J. Phys. Chem. A* **2012**, *116*, 8861−8872.

(37) Deo, G.; Wachs, I. E. Predicting Molecular Structures of Surface Metal Oxide Species on Oxide Supports under Ambient Conditions. *J. Phys. Chem.* **1991**, *95*, 5889−5895.

(38) Payen, E.; Kasztelan, S.; Grimblot, J.; Bonnelle, J. P. Surface Chemistry of MoO$_3$ γ-Al$_2$O$_3$ Catalysts Studied by Laser Raman Spectroscopy: Hydration and Dehydration Reactions and Generalization to other Supported Systems. *J. Raman Spectrosc.* **1986**, *17*, 233−241.

(39) Hu, H.; Wachs, I. E.; Bare, S. R. Surface Structures of Supported Molybdenum Oxide Catalysts: Characterization by Raman and Mo L$_3$-Edge XANES. *J. Phys. Chem.* **1995**, *99*, 10897−10910.

(40) Brandhorst, M.; Cristol, S.; Capron, M.; Dujardin, C.; Vezin, H.; Le Bourdon, G.; Payen, E. Catalytic Oxidation of Methanol on Mo/Al$_2$O$_3$ Catalyst: An EPR and Raman/Infrared Operando Spectroscopies Study. *Catal. Today* **2006**, *113*, 34−39.

(41) Hardcastle, F.; Wachs, I. Determination of Molybdenum-Oxygen Bond Distances and Bond Orders by Raman Spectroscopy. *J. Raman Spectrosc.* **1990**, *21*, 683−691.

(42) Cornac, M.; Janin, A.; Lavalley, J. C. Structure of Mo Catalysts Supported on Silica: IR and Gravimetric Results. *Polyhedron* **1986**, *5*, 183−186.

(43) Payen, E.; Grimblot, J.; Kasztelan, S. Study of Oxidic and Reduced Alumina-Supported Molybdate and Heptamolybdate Species by In Situ Laser Raman Spectroscopy. *J. Phys. Chem.* **1987**, *91*, 6642−6648.

(44) Py, M. A.; Maschke, K. Intra- and Interlayer Contributions to the Lattice Vibrations in MoO$_3$. *Physica B+C* **1981**, *105*, 370−374.

(45) Py, M. A.; Schmid, P. E.; Vallin, J. T. Raman Scattering and Structural Properties of MoO$_3$. *Il Nuovo Cimento B Series 11* **1977**, *38*, 271−279.

(46) Sleight, A. W.; Brixner, L. H. A new Ferroelastic Transition in some Al$_2$(MO$_4$)$_3$ Molybdates and Tungstates. *J. Solid State Chem.* **1973**, *7*, 172−174.

(47) Tsilomelekis, G.; Boghosian, S. On the Configuration, Molecular Structure and Vibrational Properties of MoOx Sites on Alumina, Zirconia, Titania and Silica. *Catal. Sci. Technol.* **2013**, *3*, 186−1888.

(48) Beale, A. M.; Sankar, G. In Situ Study of the Formation of Crystalline Bismuth Molybdate Materials under Hydrothermal Conditions. *Chem. Mater.* **2003**, *15*, 146−153.

(49) Leliveld, R. G.; van Dillen, A. J.; Geus, J. W.; Koningsberger, D. C. A Mo-K Edge XAFS Study of the Metal Sulfide-Support Interaction in (Co)Mo Supported Alumina and Titania Catalysts. *J. Catal.* **1997**, *165*, 184−196.

(50) Tougerti, A.; Berrier, E.; Mamede, A.-S.; La Fontaine, C.; Briois, V.; Joly, Y.; Payen, E.; Paul, J.-F.; Cristol, S. Synergy between XANES Spectroscopy and DFT to Elucidate the Amorphous Structure of

Heterogeneous Catalysts: TiO$_2$-Supported Molybdenum Oxide Catalysts. *Angew. Chem., Int. Ed.* **2013**, *52*, 6440−6444.

(51) Briois, V.; Lagarde, P.; Brouder, C.; Sainctavit, P.; Verdaguer, M. Multiple-Scattering Calculations on a Series of M(H$_2$O)$_6^{2+}$ Complexes with M = V to Cu. *Phys. B* **1995**, *208-209*, 51−52.

(52) Sakane, H.; Muñoz-Paez, A.; Diaz-Moreno, S.; Martinez, J. M.; Pappalardo, R. R.; Sanchez Marcos, E. Second Hydration Shell Single Scattering versus First Hydration Shell Multiple Scattering in M(H$_2$O)$_6^{3+}$ EXAFS Spectra. *J. Am. Chem. Soc.* **1998**, *120*, 10397−10401.

(53) Tan, X.; Fang, M.; Ren, X.; Mei, H.; Shao, D.; Wang, X. Effect of Silicate on the Formation and Stability of Ni-Al LDH at the γ-Al$_2$O$_3$ Surface. *Environ. Sci. Technol.* **2014**, *48*, 13138−13145.

(54) del Arco, M.; Malet, P.; Trujillano, R.; Rives, V. Synthesis and Characterization of Hydrotalcites Containing Ni(II) and Fe(III) and their Calcination Products. *Chem. Mater.* **1999**, *11*, 624−633.

(55) Areán, C. O.; Viñuela, J. S. D. Structural Study of Copper-Nickel Aluminate (Cu$_x$Ni$_{1-x}$Al$_2$O$_4$) Spinels. *J. Solid State Chem.* **1985**, *60*, 1−5.

(56) Payen, E.; Dhamelincourt, M. C.; Dhamelincourt, P.; Grimblot, J.; Bonnelle, J. P. Study of Co(or Ni)-Mo Oxide Phase Transformation and Hydrodesulfurization Catalysts by Raman Microprobe Equipped with New Cells. *Appl. Spectrosc.* **1982**, *36*, 30−37.

(57) The data augmentation was used in order to overcome an intrinsic limitation of the MCR-ALS method known as the rank-deficiency data issue. This issue arises when, upon chemical reaction, species are decomposed at almost the same rates, making difficult their separation by MCR-ALS and then further identification. We were facing this rank-deficiency data issue when treating the time-resolved data set recorded upon sulfidation of the as-prepared dehydrated oxidic NiMo precursor, as it will be fully discussed in a forthcoming paper.

(58) Ruckebusch, C.; Blanchet, L. Multivariate Curve Resolution: A Review of Advanced and Tailored Applications and Challenges. *Anal. Chim. Acta* **2013**, *765*, 28−36.

(59) O'Neill, H. S. C.; Dollase, W. A.; Ross, C. R. Temperature Dependence of the Cation Distribution in Nickel Aluminate (NiAl$_2$O$_4$) Spinel: a Powder XRD Study. *Phys. Chem. Miner.* **1991**, *18*, 302−319.

(60) Kelly, S. D.; Yang, N.; Mickelson, G. E.; Greenlay, N.; Karapetrova, E.; Sinkler, W.; Bare, S. R. Structural Characterization of Ni-W Hydrocracking Catalysts Using In Situ EXAFS and HRTEM. *J. Catal.* **2009**, *263*, 16−33.

(61) Cairns, R. W.; Ott, E. X-Ray Studies of the System Nickel-Oxygen-Water. I. Nickelous Oxide and Hydroxide. *J. Am. Chem. Soc.* **1933**, *55*, 527−533.

(62) Plazenet, G.; Cristol, S.; Paul, J.-F.; Payen, E.; Lynch, J. Sulfur Coverage and Structural Disorder in γ-alumina-supported MoS$_2$ Crystallites: an In Situ EXAFS Study. *Phys. Chem. Chem. Phys.* **2001**, *3*, 246−251.

(63) Van Loon, L. L.; Dutton, M. D.; Throssell, C. Comparison of Nickel Speciation in Workplace Aerosol Samples using Sequential Extraction Analysis and X-ray Absorption Near-edge Structure Spectroscopy. *Environ. Sci. Process. Impacts.* **2015**, *17*, 922−931.

(64) Marini, C.; Joseph, B.; Caramazza, S.; Capitani, F.; Bendele, M.; Mitrano, M.; Chermisi, D.; Mangialardo, S.; Pal, B.; Goyal, M. Local Disorder Investigation in NiS$_{2-x}$Se$_x$ using Raman and Ni K-edge X-ray Absorption Spectroscopies. *J. Phys.: Condens. Matter* **2014**, *26*, 452201.

(65) Hamabe, Y.; Jung, S. B.; Suzuki, H.; Koizumi, N.; Yamada, M. Quasi In Situ Ni K-edge EXAFS Investigation of the Spent NiMo Catalyst from Ultra-deep Hydrodesulfurization of Gas Oil in a Commercial Plant. *J. Synchrotron Radiat.* **2010**, *17*, 530−539.

(66) Koizumi, N.; Hamabe, Y.; Jung, S. B.; Suzuki, Y.; Yoshida, S.; Yamada, M. In Situ Observation of Ni-Mo-S Phase Formed on NiMo/Al$_2$O$_3$ Catalyst Sulfided at High Pressure by Means of Ni and Mo K-edge EXAFS Spectroscopy. *J. Synchrotron Radiat.* **2010**, *17*, 414−424.

(67) Bouwens, S. M. A. M.; Van Veen, J. A. R.; Koningsberger, D. C.; De Beer, V. H. J.; Prins, R. EXAFS Determination of the Structure of Cobalt in Carbon-supported Cobalt and Cobalt-Molybdenum Sulfide Hydrodesulfurization Catalysts. *J. Phys. Chem.* **1991**, *95*, 123−134.

(68) Louwers, S. P. A.; Prins, R. Ni EXAFS Studies of the Ni-Mo-S Structure in Carbon-Supported and Alumina-supported Ni-Mo Catalysts. *J. Catal.* **1992**, *133*, 94−111.

(69) Le Bihan, L. Synthèses par Méthode Sol-Gel de Catalyseurs d'Hydrotraitement. PhD thesis, University of Lille, France, 1997.

(70) Carrier, X.; Marceau, E.; Che, M. Physical Techniques and Catalyst Preparation: Determining the Interactions of Transition-metal Complexes with Oxide Surfaces. *Pure Appl. Chem.* **2006**, *78*, 1039−1055.

(71) Lamonier, C.; Soogund, D.; Mazurelle, J.; Blanchard, P.; Guillaume, D.; Payen, E. Origin of the Dispersion Limit in the Preparation of Ni(Co) Mo/Al$_2$O$_3$ and Ni(Co)Mo/TiO$_2$ HDS Oxidic Precursors. *Stud. Surf. Sci. Catal.* **2006**, *162*, 713−720.

(72) d'Espinose de la Caillerie, J.-B.; Kermarec, M.; Clause, O. Impregnation of gamma.-Alumina with Ni(II) or Co(II) Ions at Neutral pH: Hydrotalcite-Type Coprecipitate Formation and Characterization. *J. Am. Chem. Soc.* **1995**, *117*, 11471−11481.

(73) de Bokx, P. K.; Wassenberg, W. B. A.; Geus, J. W. Interaction of Nickel Ions with a γ-Al$_2$O$_3$ Support During Deposition From Aqueous Solution. *J. Catal.* **1987**, *104*, 86−98.

(74) Reinhoudt, H. R.; Crezee, E.; van Langeveld, A. D.; Kooyman, P. J.; van Veen, J. A. R.; Moulijn, J. A. Characterization of the Active Phase in NiW/γ-Al$_2$O$_3$ Catalysts in Various Stages of Sulfidation with FTIR(NO) and XPS. *J. Catal.* **2000**, *196*, 315−329.

(75) Puxley, D. C.; Kitchener, I. J.; Komodromos, C.; Parkyns, N. D. The Effect of Preparation Method upon the Structures, Stability and Metal/Support Interactions in Nickel/Alumina Catalysts. *Stud. Surf. Sci. Catal.* **1983**, *16*, 237−271.

(76) Millange, F.; Walton, R. I.; O'Hare, D. Time-resolved In Situ X-ray Diffraction Study of the Liquid-phase reconstruction of Mg-Al-carbonate Hydrotalcite-like Compounds. *J. Mater. Chem.* **2000**, *10*, 1713−1720.

(77) Rives, V. Characterisation of Layered Double Hydroxides and their Decomposition Products. *Mater. Chem. Phys.* **2002**, *75*, 19−25.

(78) Kowalik, P.; Konkol, M.; Kondracka, M.; Próchniak, W.; Bicki, R.; Wiercioch, P. Memory Effect of the CuZnAl-LDH Derived Catalyst Precursor - In Situ XRD Studies. *Appl. Catal., A* **2013**, *464-465*, 339−347.

(79) Mészáros, S.; Halász, J.; Kónya, Z.; Sipos, P.; Pálinkó, I. Reconstruction of Calcined MgAl- and NiMgAl-layered Double Hydroxides during Glycerol Dehydration and their Recycling Characteristics. *Appl. Clay Sci.* **2013**, *80−81*, 245−248.

(80) Klemkaite, K.; Prosycevas, I.; Taraskevicius, R.; Khinsky, A.; Kareiva, A. Synthesis and Characterization of Layered Double Hydroxides with Different Cations (Mg, Co, Ni, Al), Decomposition and Reformation of Mixed Metal Oxides to Layered Structures. *Cent. Eur. J. Chem.* **2011**, *9*, 275−282.